The dystrophin-glycoprotein complex in the development of *Nematostella vectensis:* Expression analyses and generation of a mutant by genome editing

By Susanne Grønnestad Velde

This thesis is submitted in partial fulfilment of the requirements for the degree of

Master of Science

Department of Biological Sciences

Faculty of Mathematics and Natural Sciences

University of Bergen

December 2021

Acknowledgments

The work presented in this thesis was carried out at the Sars International Centre for Marine Molecular Biology and the Department of Biological Science, University of Bergen.

There are many people that contributed to this project, but most of all I would like to thank my main supervisor, Fabian Rentzsch, and my co-supervisor, Natascha Bartsch. Fabian, thank you for giving me the opportunity to work with this interesting project. I have really appreciated how you always go the extra mile to take care of your master students with regular check-up meetings and Wednesday-lectures (with cake of course). You inspire me with your passion for science and your joy of teaching. Thank you for always finding time for me when I show up at your office. I would like to especially thank Natascha for teaching me everything in the lab. Thank you for always being so patient and kind, and for always trying to answer my many questions. You have thought me so much, and I could not have done this without you.

It has been an amazing experience to be part of the Rentzsch lab, especially considering the wonderful people I have gotten to work alongside. Alexis, thank you for being the big-siss in the lab, always happy to help whenever you can. James, you are a "wandering encyclopedia" (as we say in Norway), with knowledge about everything. A big thanks to Henriette for knowing everything about lab-work and always lending a helpful hand. Thank you to Eileen for taking care of all the animals, to Fatemeh for our nice conversations, and to Ivan and Quentin for making me feel welcome. Thank you also to my fellow master students Astrid, Mark and Linda, for your friendship and our great laughs. I would also like to thank the wonderful people at Sars and the 5th floor, for a great working environment.

A huge thanks to my friends from "lesesalen", for your friendship and all the fun times we have had at our second home (this includes Lill and Grethe for always helping us and greeting us with a smile). My roomies, Lise and Helene, I can't tell you enough how amazing it has been to live with you, and I really appreciate your friendship and support.

Finally, I would like to thank my family for being my rock. Thank you for always making time for my phone calls (almost daily), and for trying to give me advice even when you have no clue what I'm talking about and can never seem to learn how to pronounce "molecular biology". I would have never gotten this far without your love and support.

Thank you, tusen takk!

Susanne Grønnestad Velde Bergen, December 2021

Table of Contents

Selected abbreviations

AChR – Acetylcholine receptor

Ash – Achaete scute

Ath – Athonal

B4GALT – β1,4-galactosyltransferase

bHLH – Basic helix-loop-helix

CNS – Central nervous system

DG – Dystroglycan

DGC – Dystrophin-glycoprotein complex

Dpf – Day's post fertilization

ECM – Extracellular matrix

ER – Endoplasmic reticulum

Fox – Forkhead box

GABA – γ-aminobutyric acid

GlcA – Glucuronic acid

GlcNAc – N-acetylglucosamine

Hpf – Hour's post fertilization

IP – Intermediate progenitor

ISH – *In situ* hybridization

dFISH – Double fluorescence *in situ* hybridization

sgRNA – Single guide RNA

RT – Room temperature

ON – Over night

MEB – Muscle-eye-brain disease

NEC – Neuro-epithelium cell

NMJ – Neuromuscular junction

NPC – Neural progenitor cell

PNS – Peripheral nervous system

POMGNT – Protein O-linked-mannose beta-1,2-N-acetylglucosaminyltransferase

POMT – Protein O-mannosyl-transferase

POU – Pit-1, Oct-1, Unc-86

RGC – Radial progenitor cell

SGC – Sarcoglycan complex

Sox – Sry-box transcription factors

WWS – Walker-Warburg syndrome

α-DG – α-dystroglycan

β-DG – β-dystroglycan

Abstract

The development and function of cells in the nervous system and the musculature require regulated interactions with the extracellular matrix. The dystrophin-glycoprotein complex is an important regulator of these interactions. A central component of this complex is dystroglycan, a membrane protein that is heavily glycosylated on its extracellular part. This glycosylation is initiated by *O*-mannosyltransferases and is then expanded by a series of additional glycosyltransferases. The sea anemone *Nematostella vectensis* represents an evolutionary ancient group of animals and has emerged as a powerful tool to study neurogenesis and development in an evolutionary context. The genome of *Nematostella* encodes all members of the dystrophin-glycoprotein complex, introducing the question of their role in this animal. In this study, we show that the expression pattern of *dystroglycan* and five glycosyltransferases are compatible with different roles of dystroglycan *O*-mannosylation. By *in-situ* hybridization, we identified *POMGNT1, POMT1* and *POMT2* to display a similar expression pattern throughout early development. Double fluorescence *in-situ* hybridization shows the enzymes to be co-expressed with each other, suggesting a shared function. Difference in early expression between the glycosyltransferases and *dystroglycan* might indicate a dystroglycan-independent function of *O*-mannosylation, whereas the similar expression in later stages indicate a potential role for dystroglycan-dependent *O*-mannosylation during *Nematostella* development. Furthermore, double fluorescence *in-situ* hybridization found *POMGNT1* to be expressed in *FoxQ2d*-expressing sensory cells, suggesting the enzyme to have a role in sensory cells. Finally, CRISPR/Cas9 was successfully used to introduce a mutation in the gene of *POMGNT1*, to further study the function of this glycosyltransferase and its substrate in *Nematostella* development. We anticipate this study to be a starting point for future studies to provide insight on the role of the dystrophin-glycoprotein complex and the necessity of α-dystroglycan *O*-mannosylation on the nervous and muscular systems of *Nematostella vectensis*.

1. Introduction

1.1 Neurogenesis

The nervous system is a highly complex system that regulates and coordinates body functions through neurons organized into interconnected circuits. Neurons are highly polarized cells with a generally shared morphology consisting of the cell body containing the nucleus, branching cell processes called dendrites which receive signals, and an axon that conducts electrical signals which are passed along to the next neuron via synapses located at the axon termini or along the axon. Despite these general features, neurons are highly specialized and very diverse cells with many different branching patterns of their processes when fully differentiated (Lodish H, 2016).

The development of the central nervous system (CNS) of vertebrates is an often studied and comparably well understood example of neurogenesis. The CNS is precisely regulated and consists of two major parts: the brain and the spinal cord, which receives signals from the peripheral nervous system (PNS), processes the information and gives instructions to the organs of the body (Zhao et al., 2019). In vertebrates, the nervous system arises almost exclusively from the neuroectoderm part of the ectoderm. The ectoderm is formed during gastrulation and is typically divided into a neuroectoderm and a non-neural ectoderm layer. When neurogenesis begins, the ectoderm is already patterned along the anterior-posterior and the dorsal-ventral axes. Depending on the axial position, different parts of the neuroectoderm give rise to the different parts of the nervous system. By induction from the mesoderm-derived notochord, the dorsal ectoderm will form the neural plate, while the lateral parts of the neural plate will give rise to the neural crest. The neural plate will eventually develop into the CNS by invaginating and fusing to form the neural tube, with the more anterior region of the neural tube forming the forebrain, and the more posterior region forming the midbrain, hindbrain and spinal cord. The neural crest cells will act as the progenitors for the peripheral nervous system (Hrdina, 1996). The non-neural ectoderm at the lateral margins of the neural plate will give rise to the epidermis (Lee and Jessell, 1999; Squire et al., 2008). Ectodermal cells with the potential to generate neural cells mark the beginning of neurogenesis (Hartenstein and Stollewerk, 2015).

In vertebrates, neurogenesis usually starts with a self-renewing neural stem cell with the ability to proliferate and generate neurons and glia cells. The neural tube wall consists of highly polarized neuro-epithelial cells (NECs) that will turn into radial glial progenitor cells (RGCs) when the formation of neurons commences (Paridaen and Huttner, 2014). The stem cells can undergo mitosis and give rise to a neural progenitor cell, that is either multipotent or unipotent. RGCs will first undergo symmetric cell divisions, where the resulting daughter cells are identical in size and shape. With a switch to asymmetric cell division, the RGCs will give rise to two daughter cells with different shape, size, or distribution of intrinsic molecular factors (Paridaen and Huttner, 2014). In certain areas of the brain, the RGCs give rise to an intermediate progenitor (IP) which will mainly undergo symmetric division, yielding two neurons. These RGCs will indirectly or directly generate all neurons and glial cells during neurogenesis (Paridaen and Huttner, 2014).

At the last step of neurogenesis, the new-born neurons migrate to their specific location where they mature. The axon and dendrites will grow from the neuron and establish synaptic connections. These projections are necessary for interaction and the transfer of information between the host cell to other neurons, muscles, and glands (Alberts B, 2002; Lovinger, 2008). Neurons are typically classified into three types based on this interaction: interneurons connect neurons to other neurons; motor neurons connect the brain and spinal cord to the rest of the body to control organs, mainly muscle and glands; and sensory neurons respond to stimuli and transmit them to the brain. The extracellular matrix which is secreted by both neurons and glia, has been found to have an important role in the nervous system by regulating proliferation, migration, formation of axons and the synapses, and by maintaining stability in neurons and the nervous system (Barros et al., 2011; Long and Huttner, 2019). Expression of specific genes involved in neurotransmission and in the development of specific projection patterns will define the terminal identity of the individual types of neurons (Hobert and Kratsios, 2019; Tournière et al., 2020).

1.2 Cnidaria

As genome sequencing has become more accessible, the variety of organisms being used for research is increasing (Lodish H, 2016). Cnidaria are a group of mostly marine animals that is the sister group to the Bilateria with a very long evolutionary distance to vertebrates (Telford et al., 2015). They are regarded as one of the first groups of organisms in evolution possessing a nervous system and are therefore interesting for studies on neurogenesis (Watanabe et al., 2009). By comparing neurogenesis in cnidarians to vertebrates and other bilaterians, we can better understand the evolution of neurogenesis and core aspects of this developmental process. Similarities in neurogenesis in early branching taxa likely reflect central principles that have been conserved throughout evolution. The high neurogenic potential of cnidarians (described in more detail below) is an additional developmental feature that makes them interesting for studies on nervous system formation (Galliot and Schmid, 2002).

Cnidaria consist of two clades that separated early during the evolution, the Anthozoa and the Medusozoa. The Anthozoa consist of two main subclasses, the Hexacorallia and Octocorallia, distinguished by their difference in symmetry (Figure 2.1 A) (Kelava et al., 2015). Hexacorallia, which include sea anemones, stony corals and zoanthids, are characterized by a six-fold symmetry, while Octocorallia have an eight-fold symmetry and include soft corals, sea pens and gorgonias. Medusozoa contain four classes: Hydrozoa, Scyphozoa, Staurozoa, and Cubozoa, which are distinguished from the Anthozoa clade by a medusa stage in the life cycle (Galliot and Schmid, 2002). Sessile polyps are present in both clades and can bud to give rise to the sexually reproducing medusa or reproduce sexually (in Anthozoa). Cnidarian polyps have a tube like shape with tentacles surrounding the single body opening (Rentzsch et al., 2017). As opposed to the triploblastic bilaterians with three germ layers, cnidarians are diploblastic, with the presence of only two germ layers, the ectoderm and the mesendoderm. Both germ layers are separated by the mesoglea, which is composed of extracellular matrix that resembles the basement membrane in mammals (Holstein et al., 2003; Technau and Steele, 2011). The mesendodermal and the ectodermal nervous systems are made up of three classes of cells called epithelial sensory cells, ganglion cells and cnidocytes. The cnidarian nervous system has been described as a net of different neuron densities, where the anthozoan polyp often displays accumulation of neurites along the mesendodermal folds that

extends from the body wall into the gastric cavity, called mesenteries (Nakanishi et al., 2012). Cnidarians have developed into a well-established group of model organisms to investigate the evolution of the nervous system and animal development. As an addition to the well-established model organism *Hydra,* the anthozoan sea anemone *Nematostella vectensis* has emerged as one of the most developed and used cnidarian model for developmental research (Layden et al., 2016; Putnam et al., 2007).

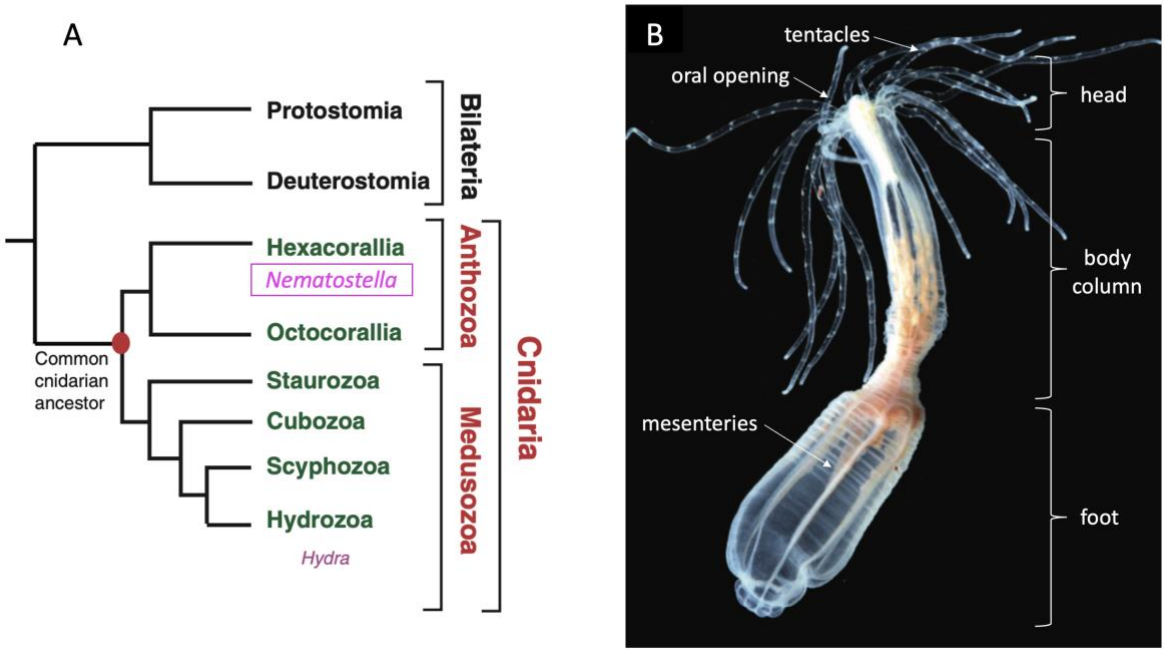

Figure 2.1: Phylogenetic tree showing the position of *Nematostella* within cnidarians and a picture of an adult *Nematostella*. (A) The phylogenetic tree places *Nematostella* in the subclass Hexacorallia within the Anthozoa clade of cnidarians. The red dot indicates the two main divisions of Cnidaria, Anthozoa and Medusozoa. The subclasses within the two clades are indicated in green, while pink indicates the two well-established model organisms within their clade, where *Nematostella* is marked with a box. Figure modified from (Technau and Steele, 2011). **(B)** adult *Nematostella vectensis* with indicated anatomic features. Figure modified from (Layden et al., 2016).

1.3 *Nematostella vectensis* as model organism

The last two decades have introduced significant research on *Nematostella* as a model system after the publication of a protocol in 1992 describing how to maintain the complete life cycle of *Nematostella* in culture (Hand and Uhlinger, 1992). The sea anemone is euryhaline and has its natural habitat in brackish water on the south coast of England and on the American Atlantic and Pacific coasts (Darling et al., 2004). The tube-like contracting body column can reach a length ranging from 1 cm up to 10 cm, depending on the animal being in its natural habitat or kept in laboratory conditions (Darling et al., 2004; Steinmetz et al., 2017). The

primary body axis, the oral-aboral axis, stretches from the oral opening to the aboral end, while the secondary directive axis runs orthogonal to the oral-aboral axis (Layden et al., 2016). In nature, the aboral part of the body column, the physa, is typically buried in mud with the single oral opening at the capitulum (head) surrounded by up to 16 prey-catching tentacles (Figure 2.1 B) (Williams, 1975). The tentacles are continuous with a pharynx and eight mesendodermal infoldings called mesenteries that run along the oral-aboral axis of the body column (Figure 2.1 B and Figure 2.2 A-D) (Renfer et al., 2010). The gametogenic area, the somatic gonad, where the germ cells develops, are located between the retractor muscle and the septal filaments (Figure 2.2 D) (Moiseeva et al., 2017). The retractor muscle on the mesenteries and the ciliated groove on one side of the pharynx, corresponds to the anthozoan internal bilaterality (Technau and Steele, 2011).

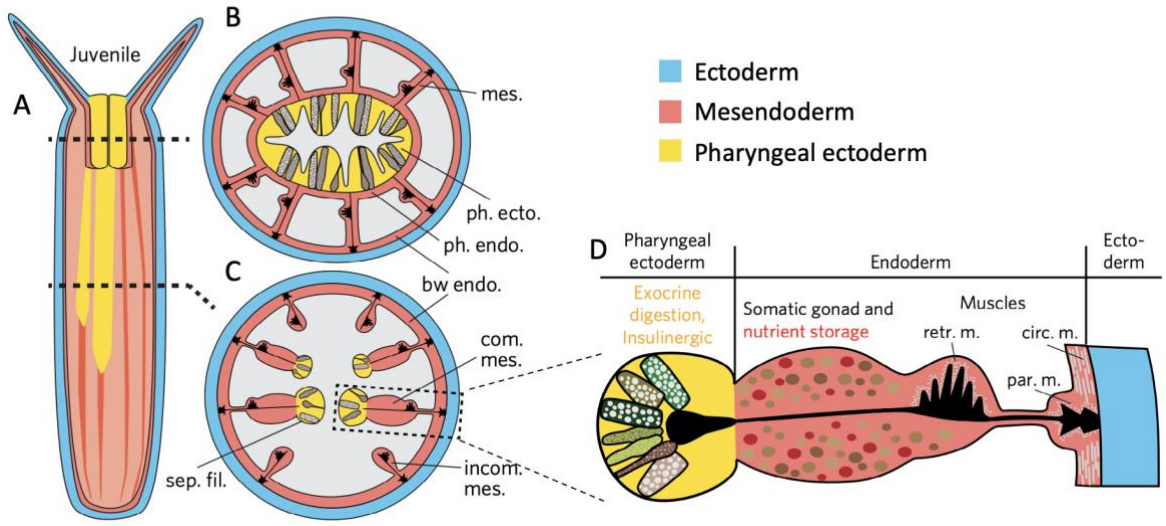

Figure 2.2: Schematic drawing and cross-section of a juvenile *Nematostella*. (A) A juvenile animal with the different germ layers and cross sections to show the body column with the mesenteries. **(B)** The upper cross-section shows the pharynx (yellow) with the two germ layers (blue, red) and the distribution of the eight mesenteries. **(C)** The lower cross-section indicates the complete and incomplete mesenteries that runs along the oral-aboral axis. **(D)** A close-up shows the cross-section of a complete mesentery with its components. The endodermal part consists of the different types of muscles, the somatic gonad and the nutrients storage. The septal filament of the pharyngeal ectoderm contains the exocrine and insulinergic cells that participates in the digestion. bw, body wall; circ. m., circular muscle; com. mes., complete mesentery; ecto., ectoderm; endo., endoderm; incom. mes., incomplete mesentery; par. m., parietal muscle; ph., pharynx; retr. m., retractor muscle; sep. fil., septal filament. Figure modified from (Steinmetz et al., 2017).

1.3.1 Life cycle of *Nematostella*

Nematostella are dioecious, meaning female and male reproductive organs are carried by different individuals, and after spawning the fertilization will happen externally. In culture, female spawning can be induced by a temperature and light shift, stimulating the formation of gametes in the mesenteries (Fritzenwanker and Technau, 2002). When squeezed through the epithelium of the mesenteries into the gastric cavity, the eggs are covered in a gelatinous jelly to form egg packages to be released out of the oral opening. Male *Nematostella* releases free-swimming sperm for the external fertilization (Figure 2.3 A) (Hand and Uhlinger, 1992). Once fertilized with the free-swimming sperm from the males, the zygote starts a series of cleavages where the first two divisions originate at the animal pole, indicated by the position of the female pronucleus. With a delayed cytokinesis, the blastomeres are fully visually separated at the 8-cell stage and lack polarity as the nuclei is located at the center of the cells. When epithelialization occurs between the 16- and 32-cell stage, the embryos gain polarity with the translocation of the nuclei to the apical surfaces of the cells, and the development of the blastula occurs approximately between 7 and 12 hours post fertilization (hpf) (Fritzenwanker et al., 2007; Lee et al., 2007). Gastrulation happens with a series of invagination cycles leading to the formation of a pre-mesendodermal plate flattening at the animal pole. The mesendodermal cells will make adhesion contact with the basal side of the blastoderm, and the embryo will become bilayered at 20-26 hpf with a mesendoderm- and ectoderm germ layer (Figure 2.3 B). The extended blastoporal lip will develop to become the pharynx and the ectodermal septal filament at the tip of the mesenteries during the planula stage (Steinmetz et al., 2017; Technau, 2020). The planula larva will be free swimming until metamorphosis and the formation of tentacle buds and tentacles take place at primary polyp stage at approximately 6 days post fertilization (dpf). The polyp will continue growing with access to nutrients, until sexual maturity is reached after approximately 12 weeks in culture. The life cycle is then completed, and the animals can reproduce sexually (Figure 2.3) (Layden et al., 2016).

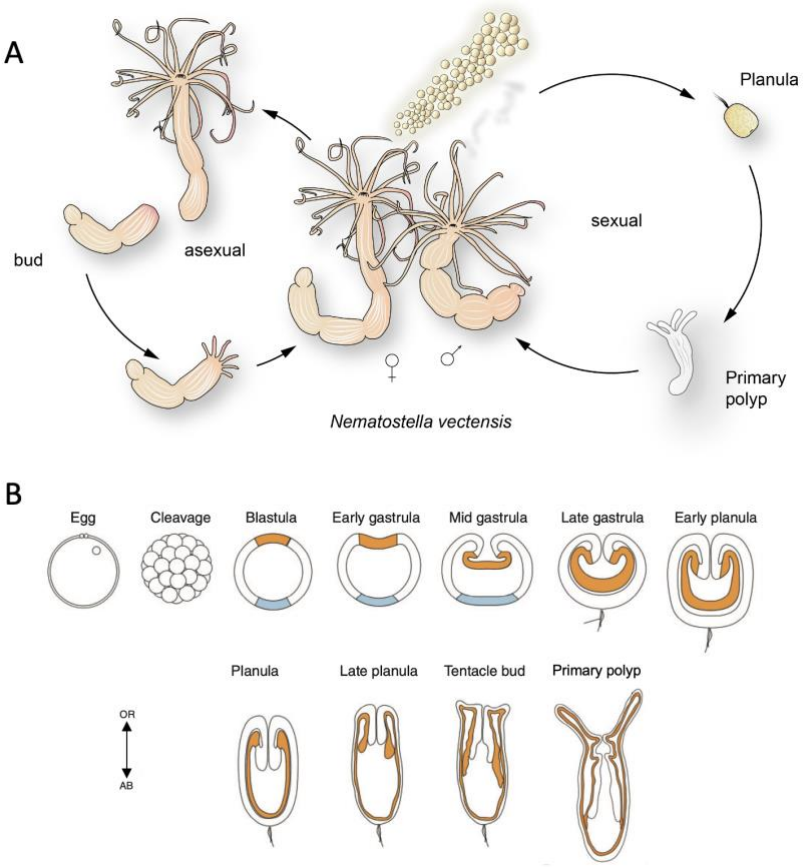

Figure 2.3: Schematic displays of the lifecycle and development of *Nematostella vectensis*. (A) Adult *Nematostella* will release gametes for external fertilization, and after approx. 48-96 hpf the animal will develop into a free-swimming planula. After 6-7 days, it has reached primary polyp stage, and will continue developing until sexual maturity after approx. 3-6 months. By asexual reproduction, the adult animal will bud off the physal region which will develop into a new mature animal. The figure is modified from (Kelava et al., 2015). **(B)** The development and morphology of *Nematostella* from fertilized egg to primary polyp is displayed. The germ layers are indicated in colours where the outer ectoderm is in white, the aboral ectoderm domain in blue, and the mesendoderm indicated in orange. The animals are oriented with the oral pole upwards. The figure is modified from (Layden et al., 2016).

Nematostella also share the ability to undergo regeneration. Comparing development and regeneration in model systems has been challenging due to most model systems not being experimentally accessible for both regeneration and development. Due to the easy maintenance of the *Nematostella* life cycle in culture and the highly regenerative features, *Nematostella* is a good tool to investigate the relationship between regeneration and development (Layden et al., 2016; Röttinger, 2021). The sea anemone possesses the ability to fully regenerate from a stump of amputated tissue from the aboral physa. The stump will undergo several steps of cellular events to close the wound and continue the development of a new head containing mesenteries, pharynx and tentacles. In less than one week, the animals

are capable of regenerating the oral part and the whole body axis (Bossert et al., 2013; Layden et al., 2016). Natural regeneration occurs by transverse fission of the physa where the adult *Nematostella* will experience intense circumferential contractions through the body column. These will form a narrowing in the physal region where fission will occur and the physa will be "pinched" off (Figure 2.3 A). The physal fragment will develop mesenteries, pharynx and tentacles as with regeneration induced by amputation (Burton and Finnerty, 2009). The larger oral fragment will usually heal its wound but can in rare cases also involve a reversal of the polarity resulting in the development of a second mouth at the site of the physa. In these cases, a transverse fission between the two heads will usually occur, producing two complete polyps (Reitzel et al., 2007).

1.3.2 Neurogenesis in *Nematostella*

In contrast to most bilaterians, both the ectodermal and mesendodermal layer will generate neurons in *Nematostella.* As in other cnidarians, the nervous system contains three classes of neural cells, sensory cells, ganglion cells (comparable to interneurons) and the cnidarian specific cnidocytes, also known as stinging cells. The nervous system is described as a nerve net with accumulations of neurites along the mesenteries (Figure 2.4) (Layden et al., 2016). Neural progenitor cells (NPCs) will emerge from the single tissue layer at blastula stage, with the potential to give rise to the different neural cell types (Rentzsch et al., 2017). At gastrula stage it is suggested that NPC begin to give rise to sensory cells, ganglion cells and cnidocytes. Sensory cells and ganglion cells are distributed in the ectoderm and endoderm, whereas cnidocytes are only found in the ectoderm. At mid-planula stage sensory cells are visible in the lateral body wall ectoderm where their neurites initially project towards the aboral end. At polyp stage, the neural cells have developed connecting neurites and the nerve net is established (Figure 2.4) (Nakanishi et al., 2012; Watanabe et al., 2014).

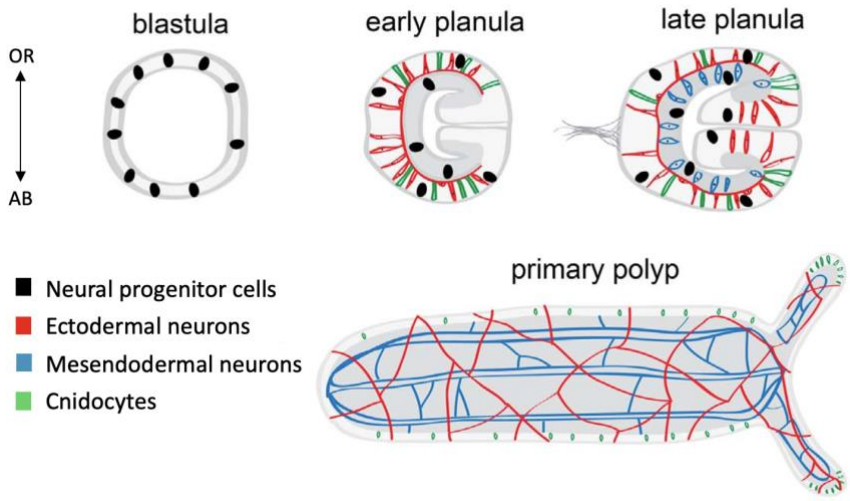

Figure 2.4: Schematic representation of the development of the nervous system in *Nematostella*. At blastula stage, NPCs will emerge from the single layer and give rise to ectodermal neurons and cnidocytes at early planula. Late planula displays the addition of mesendodermal neurons, while at primary poly stage, the neurites have formed a connecting nerve net. The animals are oriented with the oral pole to the right. The figure is modified from (Richards and Rentzsch, 2014).

Candidate gene approaches identified a remarkable level of similarity of *Nematostella* and bilaterian neurogenesis. The NPC emergence in *Nematostella* is promoted by the transcription factors *Atonal-like* and *SoxB(2).* Knockdown studies *of SoxB(2)* have shown to block the generation of all neural cell types, indicating that this gene plays an essential role in the formation of the different types of neurons (Layden et al., 2016; Richards and Rentzsch, 2014). *SoxB(2)* and *Atonal-like* expressing cells are found in a scattered pattern throughout the ectoderm and later in the mesendoderm. *AshA* is a *Nematostella* homolog of the achaete-scute family of bHLH transcription factors, which has been found to promote neurogenesis by regulating both ectodermal and mesendodermal neural development during early neurogenesis (Layden et al., 2012; Layden et al., 2016). These genes are known as “proneural genes” which trigger neural differentiation and are important for the definition of neurons and the progenitor cell fates (Hartenstein and Stollewerk, 2015; Quan and Hassan, 2005). *AshA* is expressed later in the development than *SoxB(2)* but was found to be co-expressed in non-proliferating cells, in contrast to *Atonal-like* which was found to be co-expressed with *SoxB(2)* in dividing NPCs. This suggests *Atonal-like* and *SoxB(2)* to promote neurogenesis and being involved in the specification of NPCs, while *AshA* is involved in regulation of the differentiation programs during later stages of neurogenesis (Richards and Rentzsch, 2015).

In bilaterians, the Notch signaling pathway is important in the regulation of neurogenesis. By using the γ-secretase inhibitor DAPT, studies on *Nematostella* have shown that Notch activity can regulate and suppress neural development by suppressing the expression of the *SoxB(2)* and *Atonal-like* transcription factors (Kelava et al., 2015). Knockdown of Notch gene expression using morpholinos has caused increased expression of *AshA*, while overexpression of Notch suppresses *AshA* (Layden and Martindale, 2014). These studies indicate that Notch signaling negatively regulates *Atonal-like* and *NvSoxB(2)* expressing NPCs, and thereby suppressing neural development (Layden et al., 2016; Richards and Rentzsch, 2015). Overall, the roles of Notch signaling, proneural bHLH genes and SoxB genes in *Nematostella* neurogenesis are reminiscent of their roles in bilaterian model organisms and suggest a high degree of conservation in the early stages of neurogenesis.

In *Nematostella* there is not much known about how the late steps of differentiation of neural subtypes are controlled, but some cell types can be characterized by the expression of several markers such as transcription factors or neurotransmitter receptors. For this reason, transgenic lines are generated that visualize the specific populations of neurons by the expression of a fluorescent protein. This allows to study the generation of neurons and their progeny in more detail. One example of a transgenic line which helps to understand these processes is *NvPOU4::memGFP* (Tournière, 2020). In *Nematostella POU4* acts as a terminal selector, and is expressed in post-mitotic cells derived from *SoxB(2)*-expressing NPCs. These cells give rise to cnidocytes, sensory cells and ganglion cells, where *POU4* participates in the terminal differentiation of neural cells manifesting the identity of the individual neural cell types in *Nematostella* (Tournière et al., 2020). The transcription factor *FoxQ2d* has been identified in unipotent progenitor cells derived from neural progenitor cells expressing *SoxB(2)*. The *FoxQ2d*::*mOrange* transgenic line showed that *FoxQ2d* expressing cells generate a morphologically homogenous population of putative sensory cells. While this cell population is regulated by Notch signaling and depends on expression of *Atonal-like* and *SoxB(2)*, the exact role of *FoxQ2d* is currently unclear (Busengdal and Rentzsch, 2017). In an attempt to better understand different populations of neural cells, the transcriptomes of cells isolated from different transgenic reporter lines have been generated (Gahan, Kouzel and Rentzsch, unpublished data). In the transcriptome of the cells of the *FoxQ2d::mOrange* reporter line, *POMGNT1*, coding for a glycosyltransferase, was upregulated. In mammals, this

enzyme is known to take part in the conserved *O*-mannosylation of Dystroglycan, which has roles in the development of the nervous system and the musculature. The function in *Nematostella* is not known, but we hypothesized that it might have a role in the terminal differentiation and maintenance of neural features.

1.4 *O*-mannosylation of Dystroglycan – a conserved post-translational modification

The dystrophin-glycoprotein complex (DGC) is a multiprotein complex with the main function to create and sustain a link between the extracellular matrix (ECM) and the cytoskeleton of muscle cells in a variety of mammalian tissues. The complex is also essential for maintaining the stability of neuromuscular synapses, normal development of the CNS, myelination and architecture of peripheral nerves and signal transduction (Adams and Brancaccio, 2015). Molecularly, it can be divided into three components: Dystroglycan (DG), the Sarcoglycan complex (SGC), and the cytoplasmic complex of Dystrophin, Dystrobrevins and Syntrophin (Figure 2.5 A) (Waite et al., 2012).

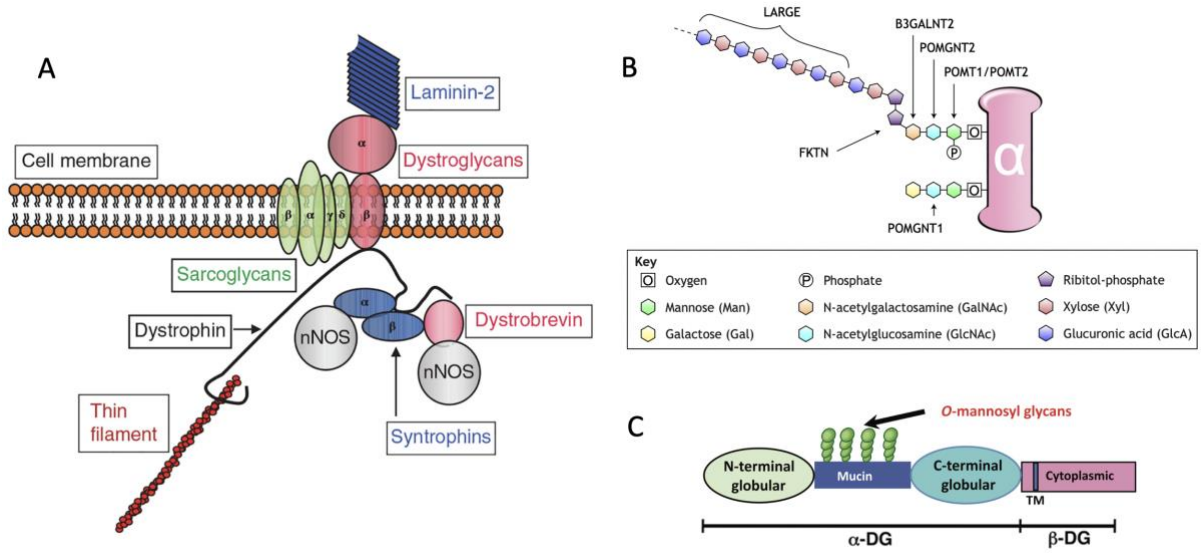

Figure 2.5: Figure representing the DGC and the glycosylation of α-DG. (A) A schematic figure showing the DGC within the cell membrane. The extracellular α-DG binds directly to laminin in the basement membrane, while β-DG is bound to actin through Dystrophin. The complex includes Dystrophin, Sarcoglycans, Dystrobrevin and Syntrophins. Nitric oxide synthase (Monzo et al.) works as a signaling molecule within the complex. **(B)** The simplified drawing shows glycosylation of α-DG where POMT1/POMT2 catalyses the first step, followed by POMGNT1 or POMGNT2 depending on the core structure. Several enzymes will continue to add to the

disaccharide chain, where LARGE will catalyse the final step. Figure modified from (Nickolls and Bonnemann, 2018). **(C)** Domain structure of Dystroglycan indicating the two subunits and the mucin-like domain which is glycosylated by the glycosyltransferases. Figure modified from (Endo, 2014)

Dystroglycan is expressed in cells of the skeletal muscle, nervous system, kidney, digestive tract, reproductive organs, and skin. The protein is composed of two non-covalently interacting subunits, α-DG and β-DG. α-DG as the extracellular part of the protein, functions as a receptor for extracellular ligands like laminin in the basement membrane, while anchored to the transmembrane β-DG, that further interacts with Dystrophin to connect to the actin cytoskeleton (Figure 2.5 A) (Adams and Brancaccio, 2015). The α-DG subunit is, under normal conditions, heavily glycosylated on serine and threonine residues at its mucin-like domain, by a series of enzymes referred to as glycosyltransferases (Figure 2.5 A-C) (Gomez Toledo et al., 2012). Glycosylation of proteins is an important post-translational modification for the function of proteins, stabilization, and cell-cell interaction. *O*-linked glycosylation, where a sugar molecule is attached to the oxygen atom of the hydroxyl group of serine of threonine, is evolutionary conserved and present in a wide range of species from bacteria to humans (Lommel and Strahl, 2009; Panin and Wells, 2014). In humans, complete lack of this modification has been found incompatible with life (Sparks, 2012).

There are three types of *O*-mannosyl glycan core structures found on α-DG: M1, M2 and M3, each with slightly different biosynthetic pathways (Imae et al., 2018). Core M1 and M2 starts with protein *O*-mannosyl-transferase 1- and 2 (POMT1 and POMT2) catalyzing the first step of glycosylation by addition of an *O*-linked mannose to the hydroxyl group of serine and threonine at the mucin-like domain of α-DG. After the first step, *O*-mannosylated dystroglycan is transported from the endoplasmic reticulum (ER) to the Golgi apparatus, where protein *O*-linked-mannose beta-1,2-N-acetylglucosaminyltransferase (POMGNT1) will transfer N-acetylglucosamine residues to the *O*-linked mannose. Fukutin is reportedly associated with POMGNT1 in the Golgi compartment, yet the exact function is unknown (Endo, 2007; Xiong et al., 2006). β1,4-galactosyltransferase 2 (B4GALT2) will add to the chain together with other transferases, but the details of these enzymes are not fully elucidated (Endo, 2014). Core M3 pathway resembles M1 and M2 with POMT1 and POMT2 catalyzing the first step but differs with the transfer of N-acetylglucosamine (GlcNAc) catalyzed by

POMGNT2. Next, β1,3-galactosyltransferase 2 (B3GALNT2), fukutin and FKRP among other transferases, add to the disaccharide chain of the α-DG in the ER, before the LARGE glycosyltransferase catalyzes the final step in the glycosylation synthesis within the Golgi apparatus by synthesizing repeats of polymers as xylose (Xyl) and glucuronic acid (GlcA) residues to the M3 chain (Figure 2.5 B). The elongated chain of disaccharides is located on the cell surface and is essential in the binding to the extracellular laminin (Endo, 2015; Nickolls and Bonnemann, 2018).

1.4.1 Diseases linked to glycosylation of α-DG

Several diseases in humans are linked to the DGC, where defective glycosylation of α-DG is implicated in several types of congenital muscular dystrophies, called dystroglycanopathies, with muscles, brain and eye abnormalities. Genetic mutations in the enzymes that modulates glycosylation of α-DG, is also a leading cause for muscular dystrophies. To date, eight genes have been shown to have an effect on the glycosylation of α-DG when mutated (Panin and Wells, 2014). As with absence of Dystroglycan, hypoglycosylation of α-DG is also associated with muscular weakness, brain malformation and intellectual disability (Adams and Brancaccio, 2015). POMGNT1, which is responsible for the second step of the α-DG glycosylation pathway, is a type II membrane protein localized in the Golgi apparatus with an C-terminus in the Golgi lumen, a transmembrane domain, a stem domain, and cytoplasmic N-terminus (Xin et al., 2015). In humans, POMGNT1 is composed of 660 amino acids with 22 identified mutations associated with the recessive muscular dystrophy muscle-eye-brain disease (MEB) (Diesen et al., 2004). Patients with this disease will display muscular dystrophy, ocular abnormalities, and brain malformation. By performing experiments targeting different mutations throughout the *POMGNT1* gene, the results suggest that the C-terminus is essential for enzymatic activity, and mutations in *POMGNT1* resulted in no enzyme activity (Manya et al., 2003). Walker-Warburg syndrome (WWS) is categorized as the most severe type of dystroglycanopathies, caused mostly by mutations in the *O*-mannosyltransferases *POMT1* and *POMT2*, but has also been found in patients with mutation in other glycosyltransferases (Table 2.1). POMT1 and POMT2 are responsible for the first catalyzing step of the *O*-mannosylation of α-DG. They have been found to co-localize in different tissues and species, and act together as a heterodimer (Ichimiya et al., 2004; Uribe et al., 2016). Mutations in

these glycosyltransferases have also been identified in patients with other types of muscular dystrophies (Table 2.1) (Hayashi et al., 2001; Sparks, 2012).

Gene	Diseases
POMGNT1	MEB WWS LGMD
POMGNT2	LGMD *
POMT1	WWS MEB LGMD
POMT2	WWS MEB LGMD
Fukutin	FCMD WWS LGMD
LARGE	MDC WWS
DAG1	LGMD

Table 2.1: An overview showing the different diseases linked to mutations in the glycosyltransferases. MEB – muscle-eye-brain disease, WWS – Walker-Warburg syndrome, LGMD – limb-gridle muscular dystrophy, FCMD – Fukuyama congenital muscular dystrophies, MDC1D – congenital muscular dystrophy type 1D. *milder form. The data is compiled from (Sparks, 2012).

1.4.2 Dystroglycan and its modifying enzymes in the brain and nervous system

Many functions have been ascribed to α-DG, but its role has mainly been studied in association with muscle integrity. In recent years, the function of Dystroglycan has also been explored for the CNS (Montanaro and Carbonetto, 2003; Nickolls and Bonnemann, 2018). The absence or disruption of basement membrane in *Dag1*-null embryonic mouse stem cells has shown that α-DG is likely to participate in the maintenance of the basement membrane throughout the whole body (Henry and Campbell, 1998). Similarly, hypoglycosylation of α-DG has been shown to disrupt the basement membrane in both muscle and brain (Grewal et al., 2001; Hayashi et al., 2001). Connection between α-DG and the basement membrane is important for proper development of the brain and the CNS. Cells proliferate in the ventricular zone of the vertebrate brain, and postmitotic neurons migrate along radial glia cells towards the marginal zone. The postmitotic neurons detach from the glia cells once they have reached their positions. α-DG is highly expressed in glial cells, and knockout of *dystroglycan* or hypoglycosylation of α-DG will disrupt the interaction between the DGC and the proteins of the basement membrane, leading to destabilization of their interaction with

the radial glia cells. Destabilized interaction can cause severe malformation and disorganization of the cortical layering, resulting in displaced neurons and glia cells that give rise to cobblestone lissencephaly, a smoothening of the brain surface and a feature in muscular dystrophies (Montanaro and Carbonetto, 2003; Nickolls and Bonnemann, 2018).

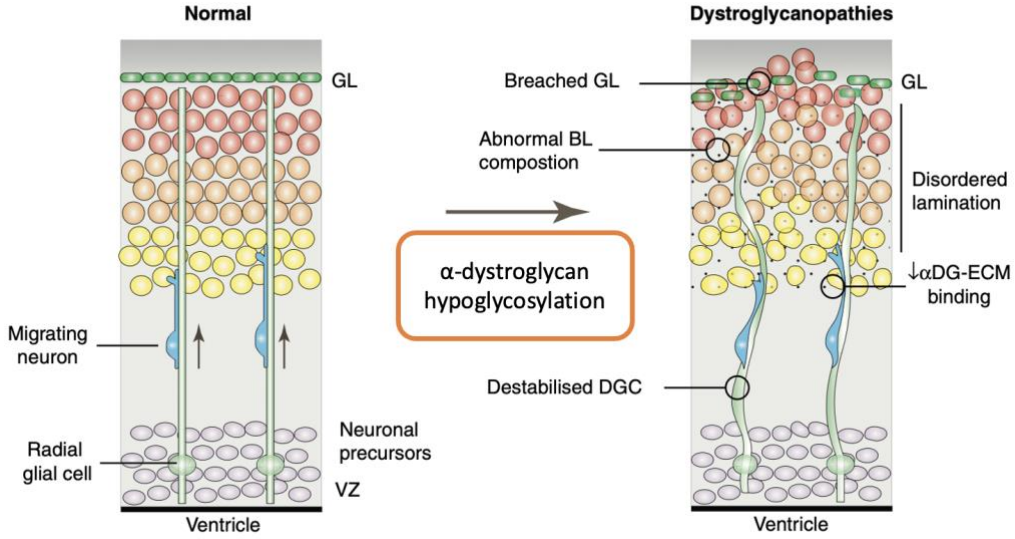

Figure 2.6: Hypoglycosylation of α-DG affects the neuronal migration in the developing cortex. Neural progenitors will migrate along radial glial cells out of the ventricular zone (VZ). Deletion or hypoglycosylation of α-DG will disrupt the binding between the DGC and the ECM, causing destabilization of the glial cells. This can cause overmigrating neurons, disordered lamination, abnormal basal lamina (BL) and breaches in the glial limitans (GL). Figure modified from (Waite et al., 2012).

The DGC has been shown to be important for the development and function of synapses in both the central and peripheral nervous system. It is required for the stability of gamma-aminobutyric (GABA) -ergic synapses in the cerebral cortex, for the clustering of acetylcholine receptors at the neuromuscular junction and for the formation of ribbon synapses in the retina. The DGC displays a central role in in the postsynaptic sites in pyramidal cells of the cerebral cortex, and Purkinje inhibitory neurons where the complex is localized at inhibitory synapses in neurons, responsible for signal transduction from one neuron to another. It colocalizes with the GABAa receptor that responds to GABA inhibitory neurotransmitters (Haenggi and Fritschy, 2006). The exact function of Dystroglycan needs further exploring, but it is believed to play a modulatory function regulating the stability of GABAergic synapses (Levi et al., 2002). In the peripheral nervous system, a-DG serves scaffolding functions by being the receptor of Agrin in neuromuscular junctions (NMJ), responsible for stimulating acetylcholine

receptor (AChR) clustering and enabling nerve-muscle contact. (McMahan et al., 1978; Nickolls and Bonnemann, 2018). Similar to the function of Dystroglycan in NMJ, it also serves a function in the synapses of photoreceptor cells in retina (Sato et al., 2008). Mutations that disrupt the glycosylation of α-DG, as mutations in *POMGNT1*, have been shown to affect the retina layers, potentially causing dystroglycanopathies that affects the eyes and sight (Sato et al., 2008; Uribe et al., 2016).

O-linked glycosylation of Dystroglycan is thus an important post-translation modification necessary for Dystroglycan to bind to its matrix ligands. As *O*-mannosylation is evolutionarily conserved, invertebrate model systems that are more amenable to genetic analysis, or that have a more simple tissue architecture, may provide valuable insights into the core functions of the dystrophin-glycoprotein complex (Panin and Wells, 2014).

1.5 Aims of the study

O-mannosylation is an essential and conserved protein modification that plays a role in the development and physiology of the nervous system in different bilaterians. The main substrate for *O*-mannosylation is the extracellular domain of Dystroglycan, which is glycosylated by several enzymes. Glycosylated Dystroglycan is necessary for stability and normal cellular function of the muscle and nervous system and mutations in the glycosyltransferases responsible for the glycosylation of α-DG have been linked to several congenital muscular dystrophies (Nickolls and Bonnemann, 2018; Wells, 2013). Some of these conserved enzymes have been identified in the genome of the cnidarian *Nematostella vectensis,* however the function of these enzymes is not yet understood. By using *Nematostella* as a model system, the aims of this study were to (1) characterize the presence and spatial localization of five enzymes participating in *O*-mannosylation as well as of their best-known substrate, α-DG, at different stages of development and (2) study the function of POMGNT1, as this enzyme was found to be upregulated in the transcriptome of a population of neural cells. To achieve this, *in situ* hybridization (ISH) was used to study the spatial expression pattern of *POMGNT1, POMGNT2, POMT1, fukutin, dystrobrevin* and *dystroglycan* throughout development, and CRISPR/Cas9 was used to generate a mutant line to study *POMGNT1* function in *Nematostella*.

2 Materials

2.1 Chemicals

Chemical	Formula /Abbrev.	Supplier	Cat. No.
4-(1,1,3,3-Tetramethylbutyl)phenyl-polyethylene glycol	Triton X-100	Sigma Aldrich	9002-93-1
4`,6-diamidino-2-phenylindole	DAPI	ThermoFisher	62248
Acetic Anhydride	$(CH_3CO)_2O$	Sigma Aldrich	45830
Agarose		Life Technologies	16500500
Bovine serum albumin	BSA	Sigma Aldrich	A4503
Citric acid	$C_6H_8O_7$	Sigma Aldrich	C0759
Diemethyl sulfoxide	DMSO	Sigma Aldrich	D8418
DIG RNA labelling mix		Sigma Aldrich	11277073910
di-Sodium hydrogen phosphate dihydrate	Na_2HPO_4 x 2 H_2O	Merck	1.06580.1000
Ethanol	CH_3CH_2OH /EtOH	Sigma Aldrich	1.00983
Ethylenediaminetetraacetic acid	EDTA	ThermoFisher	F9260G
Formaldehyde	CH_2O	Sigma Aldrich	252549
Formamide (deionized)	CH_3NO	Sigma Aldrich	F9037 / 47671
Glutaraldehyde	$C_5H_8O_2$	Sigma Aldrich	G7651
Glycerol	$C_3H_8O_3$	Sigma Aldrich	49781
Glycine	$C_2H_5NO_2$	Sigma Aldrich	50046
Heparin sodium salt		Sigma Aldrich	H3149
Hoechst 33342		ThermoFisher	62249
Hydrogen peroxide	H_2O_2	Merck	K50794709911
L-Cysteine	$C_3H_7NO_2S$	Sigma Aldrich	W326305
Lithium Chloride	LiCl	ThermoFisher	9480G
Maleic Acid	$C_4H_4O_4$ / MA	Sigma Aldrich	M0375
Methanol	CH_3OH / MeOH	Sigma Aldrich	32213
Nitro-blue tetrazolium chloride/5-bromo-4-chloro-3'-indolyphosphate p-toluidine salt	NBT/BCIP	Sigma Aldrich	11681451001
Polyethylene glycol sorbitan monolaurate	Tween20	Sigma Aldrich	P9416
Proteinase K		Sigma Aldrich	P2308
Sodium Chloride	NaCl	Sigma Aldrich	S7653
Sodium citrate tribasic dehydrate	Na citrate	Sigma Aldrich	71402

Sodium dihydrogen phosphate monohydrate	NaH_2PO_4 x H_2O	Merck	1.06346.1000
Sodium dodecyl sulfate	$CH_3(CH_2)_{11}OSO_3Na$ / SDS	Sigma Aldrich	05030
Sodium hydroxide	NaOH	Merck	1.06462.1000
Triethanolamine	$C_6H_{15}NO_3$ / TEA	Sigma Aldrich	90279

2.2 Buffers and solutions

10x PBS	**20x SSC (pH 7.0)**
18.6 mM NaH_2PO4 x H_2O	175.3 g/l NaCl
84.1 mM Na_2HPO4 x 2 H_2O	44.1 g/l Na citrate
1.75 M NaCl	

1x PBTw	**1x PBTx**	**0.1x SSCT**	**2x SSCT**
1x PBS	1x PBS	0.5% (v/v)20x SSCT	10% (v/v) 20x SSCT
0.1%(v/v) Tween20	0.2% (v/v) TritonX-100	0.4% (v/v) Tween20	0.4% (v/v) Tween20

TNTw	**TNTx**	**1x Maleic acid buffer (MAB, pH 7.5)**
0.1 M Tris-Cl pH 7.5	0.1 M Tris-Cl pH 7.5	100mM Maleic acid
0.15 M NaCl	0.15 M NaCl	150mM NaCl
0.1% Tween20	0.2% Triton X-100	

Hybridization Buffer (+)	**Hybridization Buffer (-)**
50% (v/v) Formamide	50% (v/v) Formamide
5x SSC	5x SSC
1% (v/v) SDS	1% (v/v) SDS
0.1% (v/v) Tween-20	0.1% (v/v) Tween-20
50 µg/ml Heparin	0,925%(v/v) Citric acid
100 µg/ml Salmon sperm DNA	H_2O
0,925% (v/v) Citric acid	
H_2O	

0.5 % blocking reagent/TNT for FISH	**10% blocking reagent/1x maleic acid buffer for ISH**
0.1 M Tris-Cl (pH 7.5)	10% (w/v) Blocking reagent
0.15 M NaCl	1x Maleic acid buffer
0.5 % (v/v) Blocking reagent	

Washing after antibody: PBS-Tx-BSA	**Staining buffer: NTMT**
1x PBS	100 mM NaCl

0.2% (v/v) Triton X-100
0.1% (w/v) BSA

100 mM Tris-HCl (pH 9.5)
50 mM $MgCl_2$
0.1%(v/v) Tween-20

Genomic DNA Extraction buffer

10 mM Tris-HCl (pH 8)
1 mM EDTA
25 mM NaCl
200 µg/µl Proteinase K

2.3 Commercial kits and reagents

Name	Supplier	Cat. No.	Application
Boehringer Blocking solution (BBS)	Sigma Aldrich	11096176001	Blocking for ISH
Deoxyribonucleic acid, single stranded from salmon testes	Sigma Aldrich	D9156	Hybridization buffer
EnGen® sgRNA synthesis kit, S. Pyogenes	New England BioLabs	ES3322	sgRNA synthesis
Eva Green	Biotium	31000	Melt curve
GeneRuler DNA Ladder Mix	ThermoFisher	SM0331	Agarose gel electrophoresis
Goat serum	Merck	G9023	Blocking
GoTaq® DNA polymerase	Promega	M300	PCR
MEGAscript® Kit (SP6, T7)	Ambion	11175025910	RNA synthesis
Prolong Gold (with DAPI)	ThermoFisher	P36931	Cell slide mounting
PureYield™ Plasmid Miniprep System	Promega	A1223	Nucleic Acid extraction
S.O.C. Medium	ThermoFisher	15544034	Cell transformation
SYBR Safe® DNA gel stain	Life technologies	S33102	Agarose gel electrophoresis
TaKaRa Ex Taq® DNA polymerase	Takara	RR001C	PCR
TOP10 Competent Cells	ThermoFisher	C404010	Cell transformation
TSA® Plus Blocking	Perkin Elmer	FP1012	Blocking for FISH
TSA® Plus Cyanine 3	AKOYA	NEL744001KT	FISH
TSA® Plus fluorescein	AKOYA	NEL741001KT	FISH
T4 DNA Ligase	New England BioLabs	M0202S	Ligation

T4 DNA Ligase Reaction Buffer	New England BioLabs	B0202S	Ligation
Wizard SV gel and PCR clean-up	Promega	A9281	PCR purification

2.4 Antibodies

Name	Supplier	Species	Dilution	Cat. No.
Anti-Digoxigenin-AP	Roche	Sheep	1:4000	11093274910
Anti-Digoxigenin-POD	Roche	Sheep	1:100	11207733910
Anti-Fluorescein-POD	Roche	Sheep	1:250	11426346910

2.5 Instruments

Name	Supplier	Function
C1000 Thermal Cycler	BioRad	qPCR/melt curve
Centrifuge 5415 R	Eppendorf	Centrifuge of samples
ChemiDoc XRS+	BioRad	Gel-imaging
Eclipse TE2000-U	Nikon	Injection of fertilized eggs
FemtoJet 4i + CellTram Vario	Eppendorf	Injection of fertilized eggs
FV3000 Confocal Laser Scanning Microscope	Olympus	Imaging of fluorescent ISH and immunofluorescence
Mastercycler Nexus GSX1	Eppendorf	PCR
NanoDrop™ One Microvolume UV-Vis Spectrophotometer	Thermo Scientific	Quantifying and qualifying DNA/RNA samples
Nikon eclipse E800 compound microscope w/ Nikon Digital Sight DSU3 camera	Nikon Corporation	Imaging of colorimetric ISH

2.6 Computer software

Name	Developer	Purpose
ImageJ / Fiji	(Schindelin et al., 2012)	Image viewing
Benchling	Benchling	Biology Software for making primers
C100 Manager software	BioRad	qPCR/melt curve
Image Lab 5.1	BioRad	Gel imaging

2.7 Primers

Primer	Sequences (5'-3')	Use
POMGNT1-fwd	AGCAGAAACGACAGACAACACG	Cloning gene of interest
POMGNT1-rev	CGTAATTGTCTTTGCGCATGATTTCC	Cloning gene of interest
POMGNT2-fwd	CGAAAGTTTACGCCTTGGTTCG	Cloning gene of interest
POMGNT2-rev	TGAGCCATGCATTCCAATCAAGC	Cloning gene of interest
Dystrobrevin-fwd	TCTGTACGCTTATGACAGTGATGC	Cloning gene of interest
Dystrobrevin-rev	TAGCAGCATAACGCGAGATCAGC	Cloning gene of interest
Dystroglycan-fwd	CGGACACCAAGCATATCGTTTGC	Cloning gene of interest
Dystroglycan-rev	TTATCGCTAAGACTGAATTCGAGCG	Cloning gene of interest
Fukutin-fwd	AGCAGAGAGTGCAACAAAAGTGC	Cloning gene of interest
Fukutin-rev	TGTGAATGTTTGAATGACCTCAGGC	Cloning gene of interest
POMT1-fwd	TCAGATCCACCCTTAACCATGAGC	Cloning gene of interest
POMT1-rev	GTTTCAGGGTGAGAGTGCAGC	Cloning gene of interest
POMT2-fwd	CGCAAACAGCTTGAAGTACTTAGGC	Cloning gene of interest
POMT2-rev	TGACCTGTTGCTGTTCTGGAGC	Cloning gene of interest
M13 primer Fwd	GTAAAACGACGGCCAG	Synthesis of probe template
M13 primer Rev	CAGGAAACAGCTATGAC	Synthesis of probe template
POMGNT1gRNA3	ttctaatacgactcactataGCCTACGCTGGAGGGACACCgttttagagctaga*	CRISPR/Cas9
POMGNT1gRNA5	ttctaatacgactcactata**G**ATGGACCCGCCCACTCTCGAgttttagagctaga*	CRISPR/Cas9
MeltFwd_gRNA1+3	GAGAATGGCCCGCAATATGATG	Melt curve for sgRNA3 injected animals
MeltRev_gRNA1+3	CGTGACCTGTCTTCTGCGTC	Melt curve for sgRNA3 injected animals
MeltFwd_gRNA4+5	cagGCGTAGAGCCGTCAAT	Melt curve for sgRNA5 injected animals
MeltRev_gRNA4+5	CAGGTAATGTGGCCTCCTACTC	Melt curve for sgRNA5 injected animals

*Lower-case letters at the 5' end of the primers, indicates the T7 promoter, while the lower-case letters at the 3' end indicates the 14 nucleotide overlap as stated in the EnGen 2X sgRNA Reaction Mix intructions. Upper-case letters represent the target-specific sequence.

3 Methods

3.1 Cloning of genes of interest

DNA cloning is the process where identical copies of a particular DNA fragment are generated. After inserting the fragment of interest into cloning vectors as pGEMt-easy, the vector can be introduced into a bacterial host cell and replicated along with the host cells own DNA (Lodish H, 2016). The following genes were cloned into pGEMt-Easy vector for further experiments: NVE11295 *(POMGNT1),* NVE8876 *(POMGNT2),* NVE1204 *(dystrobrevin),* NVE3206 *(dystroglycan),* NVE25189 *(fukutin),* NVE18562 (*POMT1)* and NVE19611 (*POMT2).* These sequences were identified by the host lab via reciprocal BLAST searches using human sequences as starting point (Altschul et al., 1990; Nordberg et al., 2014).

3.1.1 Amplification and purification

To amplify the DNA of interest, PCR amplification was performed using *Ex Taq (TaKaRa)*. The 25 μl PCR reaction was prepared by addition of the following components: 2.5 μl 10X *Ex Taq* Buffer, 2 μl dNTP Mixture (2.5 mM each nucleotide), 0.5 μl of each forward and reverse primer (10 mM) (Table 2.7), 0.2 μl *TaKaRa Ex Taq* Polymerase (5U/μl) and 50 ng of cDNA template (from four embryonic stages ranging from 1 to 4 days post fertilization). The PCR reaction was run with 3 min denaturation at 94°C, followed by 45 cycles of 20 s denaturation at 94°C, 20 s annealing at specific temperatures for the different primer pairs, and 1 min extension at 72°C, ending with a final 3 min extension at 72°C. To verify the size, an aliquot was run on a 1% agarose gel and the remaining reaction was purified with Wizard® SV Gel and PCR Clean-Up System. An equal amount of membrane binding solution was added to the PCR product, followed by transfer of the PCR mix to a SV Mini column in a collection tube, and centrifugation at 16 000 x g for 1 min. The Mini column was washed twice by Membrane Wash solution (700 μl and 500 μl), and the DNA was eluted with pre-heated Nuclease-free water.

3.1.2 Ligation and transformation

The purified DNA was ligated into pGEMT-Easy Vector by adding 3.5 μl of PCR reaction to 5 μl of 10x T4 DNA ligase buffer and 1 μl of T4 DNA ligase, followed by incubation for 1.5 at RT h. The ligation product was subjected to transformation into TOP10 competent cells by 30 min

incubation on ice followed by 45 s heat shock at 42°C and 2-5 min on ice. SOC medium was added to the cells to incubate for 60 min at 37°C. The transformed bacteria were plated on X-gal treated ampicillin agar plates and incubated upside down at 37°C for 20-28 hrs, then stored at 4°C.

3.1.3 Colony PCR and inoculation

To verify the presence of the genetic construct, a colony PCR was performed. The reaction was composed of 5X Flexi buffer green, 2.5 µl $MgCl_2$, 0.5 µl dNTPs (10mM), 1 µl of each primer (10mM) (table 2.7), 0.125 µl GoTaq® DNA Polymerase (25u/ml) and 14.875 µl water. The colony PCR reaction was run with 5 min denaturation at 95°C, followed by 30 cycles of 30 s denaturation at 95°C, 30 s annealing at specific temperatures for the different primer pairs, 2 min at 72°C, ending with a final 5 min extension at 72°C. To verify the size of the insert an aliquot was run on a 1% agarose gel. The colonies with successful insert were inoculated ON in 3 ml LB culture (with 100 µg/ml ampicillin) at 37°C and 200 rpm. The pellet was resuspended and purified according to PureYield™ Plasmid Miniprep system. 600 µl of bacterial culture was added to a microcentrifuge tube in addition to 100 µl Cell Lysis Buffer and inverted 6 times. 350 µl of cold Neutralization Solution was added to the tube and centrifuged for 3 min at maximum speed. The supernatant was transferred to a PureYield™ Minicolumn and placed in a Collection Tube for 15 seconds centrifugation. Flowthrough was discarded before the minicolumn was washed with 200 µl Endotoxin Removal Wash and again centrifuged for 15 seconds. A second washing step was performed with Column Wash Solution, before elution of plasmid DNA by adding 30 µl Elution Buffer, followed by 15 seconds of centrifugation. The clones were sent for sequencing performed by GENEWIZ to confirm the orientation of the sequence.

3.2 *Nematostella vectensis* culture

The *Nematostella vectensis* animals were kept in 1/3 filtered seawater (*Nematostella* medium; NM), and raised at 21°C until adults, then maintained at 18°C. Spawning was induced by exposure to light and elevated temperature as described in (Fritzenwanker and Technau,

2002). Egg packages were collected and fertilized for 25 min before de-jellying in 3% (w/v) cysteine/NM for approximately 20 min, and several washings in NM.

3.3 Fixation

For the usage of animals in gene localization methods as *in situ* hybridization (ISH), the animals must undergo fixation. This will preserve the biological tissue by terminating ongoing biochemical reactions and increasing the stability. The chemical fixative formaldehyde is widely used for fixation, and is known for low levels of shrinkage and good preservation of the cellular structure (Hobro and Smith, 2017).

Embryos at 20 hours post fertilization (hpf) (gastrula), 30 hpf (late planula), 48 hpf (early planula), 72 hpf (planula), 96 hpf (late planula) and 6 days post fertilization (dpf) (primary polyp) were fixed in ice cold 0.25% (v/v) glutaraldehyde/3.7% (v/v) formaldehyde/NM for 90s, then incubated in 3.7% (v/v) formaldehyde/PBTw at 4°C for 1 h, while slowly rotating. The fixed embryos were washed four times in PBTw, once in H_2O and then followed by dehydration in a series of methanol washes (50%, 100% (v/v)) before final storage in 100% methanol at -20°C.

3.4 Probe synthesis for ISH

To detect localization of specific nucleic acid sequences within an organism by ISH, specific antisense RNA probes must be constructed for each sequence. The samples are hybridized with the specific digoxigenin (DIG) labeled probes that can be bound by anti-Digoxigenin antibodies coupled to alkaline phosphatase (AP). The AP activity can be detected by a black-purple color, when reacting to 5-bromo-4-chloro-3-indolyl phosphate (BCIP) and nitroblue tetrazolium salt (NBT) (Kessler, 1994).

Amplification of the template DNA by PCR was performed using ExTaq™ DNA polymerase. The 50 µl reaction consisted of ExTaq™ polymerase (6 U/µl), 5 µl 10X Ex Taq Buffer, 4 µl dNTPs (2.5 mM), 1 µl of each primer and 1 µl pGEMT-easy plasmids containing the sequence of interest. The PCR reaction was run with 3 min pre-denaturation at 94°C, followed by 45 cycles of 20 s denaturation at 94°C, 20 s annealing at 55°C, and 1 min extension at 72°C, ending with

a final 3 min extension at 72°C. An aliquot was run on a 1% agarose gel to verify the size, and purified with Wizard® SV Gel and PCR Clean-Up System, where an equal amount of membrane binding solution was added to the PCR product before it was loaded onto the column and centrifuged at 16000 x g for 1 min. Before the DNA was eluted in nuclease free H2O, the column was washed twice with wash buffer. Probe synthesis was performed with the MEGAscript® SP6/T7/T3 Kit, depending on the orientation of the insert in the plasmid. The reaction consisted of 1 µl RNA polymerase (SP6 or T7), 1.5 µl 10 X reaction Buffer (SP6/T7), 2 µl digoxigenin-labelling (DIG) mix, and 2 µg of the purified PCR product and was left to incubate for 4-5 h at 37°C. 1µl (15U/µl) TURBO DNAse was added to the reaction, incubated for 20 min at 37°C, followed by addition of an equal amount of LiCl (7.5 M lithium chloride, 50 mM EDTA) and water, ending with ON incubation at -20°C. The RNA was purified by centrifugation for 30 min at approx. 15 000 x g (4°C), where the pellet was washed with 70% EtOH, followed by 7 min centrifugation at approx. 15 000 x g (4°C). The pellet was left to dry for approximately 15 min before resuspended in equal amounts of nuclease-free water and formamide, before the probes were stored at -20°C.

3.5 Colorimetric *in situ* hybridization (ISH)

In situ hybridization is, as mentioned above, a widely used technique to detect and localize a specific DNA or RNA sequence within an organism by means of labeled complementary probes. Different labelling methods can be used, but the non-radioactive labelling with digoxigenin has in the past decades become the more preferred method (Hua et al., 2018).

Colorimetric ISH was performed to visualize the location of the seven specific nucleic acid sequences within the *Nematostella* tissue. The fixated tissue was rehydrated through a series of MetOH/PBTw washes [75%, 50%, 25%, 0% (v/v)] before incubation with 10 µg/ml Proteinase K in PBTw for 5 min at RT. The tissue was subjected to several 5 min washes with 2 times Glycine/PBTw (4mg/ml), then 0.1% TEA/PBTw, 0.25% acetic anhydride in 0.1% TEA/PBTw, 0.50% acetic anhydride in TEA/PBTw and 3 times 5 min washes with PBTw. Refixation was completed with one 30 min 3.7% formaldehyde/PBTw incubation, and 5 times 5 min washes with PBTw. The samples were left in Hybridization solution(+) at 60°C ON, before addition of an equal amount of Hybridization solution(+) with 2 ng/µl denatured DIG-

labelled probes for a final concentration of 1 ng/µl of probe. The samples with the added probes were left to hybridize for >60 hours at 60°C. After hybridization, a series of 30 min post-hybridization washes with Hybridization solution(-) in 2X SSCT [75%, 50%, 25%, 0% (v/v)] was performed at 60°C, followed by a 0.2X SSCT wash and two washes with 0.1x SSCT. Three PBTw washes at RT were conducted before blocking with 0.5% Boehringer Blocking Solution (50% MAB, 50% PBTw) for 5 min at RT and 2 hours incubation in 1% Boehringer Blocking Solution/MAB at RT. ON incubation in 1% Boehringer Blocking Solution/MAB with 1:4000 anti-digoxigenin alkaline phosphatase (Roche) was performed, before 10 post antibody incubation washes, each for 15 min with PBS-TX-BSA. The samples were then washed with NTMT staining buffer before the signal was developed with 3.5 µl/ml of NBT/BCIP in NTMT. To stop the staining, the solution was exchanged several times with NTMT, 3 times with H_2O, before de-staining in EtOH for the removal of unspecific staining. The tissue was washed with H_2O again, followed by PBTw washes and then left in 87% glycerol to be mounted on imaging slides. The samples were imaged with a Nikon Eclipse E800 compound microscope with a Nikon Digital Sight DSU3 camera.

3.6 Double Fluorescence *in situ* hybridization (double FISH)

Detecting labeled probes with a fluorescent substrate is another labeling method for ISH, called fluorescence *in situ* hybridization (FISH). To investigate co-expression of genes, a double FISH combining both fluorescent- and DIG-labelled probes can be performed. The labeled probes can be detected by an enzyme-coupled antibody that will process a substrate into a fluorescent molecule.

Fixed tissue samples from different stages (20, 30, 48, and 72 hpf) were subjected to H_2O_2 treatment with 3% H_2O_2 in MeOH for 20 min, before rehydration, proteinase K treatment, refixation, pre-hybridization and hybridization as described under the "Colorimetric *in situ* hybridization" section. Hybridization was performed with either digoxigenin (DIG) or fluorescein isothiocyanate (FITC) labelled riboprobes at a concentration of 1 ng/µl. Post-hybridization washes at 60°C were performed as described for colorimetric ISH, before the samples were subjected to a series of post-hybridization washes at RT with 0.1x SSCT in TNTw [75%, 50%, 25%, 0% (v/v)]. The samples were blocked with 0.5% Perkin Elmer blocking

reagent in TNB for 1 h at RT, before addition of either anti-DIG-POD (1:100) or anti-Fluorescein-POD (1:250) in blocking solution and incubation at 4°C ON. Before staining, the samples were washed 10 times with TNTx, and then stained with Cyanine3 (Cy3) (1:50) in 1x working solution (TSA Plus Cyanine 3 System kit, AKOYA) for 30 min. The samples were washed in TNTw and PBT before stopping the peroxidase activity with 10 min incubation in 0.1 M glycine/0.1% tween with a pH of 2. Before the second treatment with 3% H_2O_2 in PBT, the samples were washed three times with PBT. Three TNTw washes were performed before a new blocking with 0.5% blocking in TNB and antibody incubation with either anti-DIG-POD (1:100) or anti-Fluorescein-POD (1:250) in blocking solution. 10 TNTx washes were carried out, and the samples were incubated in the dark with Fluorescein for 40 min. Washes with TNTx and PBTx were performed before nuclear staining with DAPI/PBTx (1:100, 1mg/ml) for 30 min. The staining solution was washed away with PBTx, and the samples were left in 70% glycerol/PBS to be mounted and imaged with Leica SP5 confocal microscope and processed in Imaris or ImageJ.

3.7 CRISPR/Cas9 and sgRNA synthesis

CRISPR/Cas9 is a gene editing method that exploits the abilities of the bacterial protein Cas9 to cut DNA in a controlled manner. The method requires a single guide RNA (sgRNA) that targets a specific part of the genome and guides the Cas9 to cut the DNA at this specific location. The repair system of the cell will recognize the damage and aim to repair it by Non-Homologous End Joining (NHEJ). This repair system is error prone and can induce mutations and frameshifts in the protein coding region (Driehuis and Clevers, 2017).

SgRNAs of approx. 20 bp were designed (table 2.7) by using Benchling (Benchling [Biology Software]. (2021). Retrieved from https://benchling.com) and synthesized with EnGen® sgRNA Synthesis Kit. The reaction of 5 µl EnGen 2X sgRNA Reaction Mix (*S. pyogenes*), 2.5 µl target specific designed DNA oligo (1 µM), 0.5 µl DTT (0.1 M), 1 µl EnGen sgRNA Enzyme Mix, 1 µl of nuclease free water, were incubated at 37 °C for 1 h. The reaction was put on ice and 15 µl nuclease free water and 1 µl DNase I mix was added for further incubation at 37 °C for 15 min. 16 µl LiCl was added to the reaction before incubation at -20 °C ON. The RNA was centrifuged for 30 min before the LiCl solution was carefully removed and the pellet washed

with 80% EtOH. The RNA was again centrifuged for 15 min, for removal of excess EtOH before drying the pellet by evaporation of the EtOH. At last, the pellet was resolved in nuclease free water and the concentration measured by Nanodrop.

3.7.1 Injection of sgRNA and Cas9

450 ng of the sgRNA was mixed with 1.8 µl CAS 9 enzyme (PNA Bio CP01), 1 µl Alexa488 in 1.1 M KCl and water up to 4 µl. The mix was incubated in the dark at 37°C for 5-15 min, before microinjection into fertilized eggs as described in previously published protocols (Rentzsch et al., 2020). The injected animals were kept at 21°C to grow, until genomic DNA (gDNA) extraction was performed in primary poly stage. The remaining injected animals were kept and raised to later cross to wildtype when the animals become sexual mature.

3.8 gDNA extraction and Melt curve with EvaGreen®

Genomic DNA (gDNA) was extracted from the injected animals, to perform melt curve analysis and detect possible mutations in the DNA. The technique is based on the detection and measurements of amplicons during each cycle of the amplification, by measuring the proportional increase in fluorescence signal (Prada and Castellanos, 2013). EvaGreen® dye is a DNA-binding dye that will change conformation when bound to double stranded DNA and emit fluorescence once bound. Gradual temperature increase will lead to denaturing of the PCR fragment and sudden loss of the fluorescence at the melting temperature. Mutations in the region amplified by PCR results in the presence of heteroduplexes that release the fluorescing dye at a different temperature. A derivative curve will contrast the negative derivative (-Rn') of fluorescence versus the temperature and allow for visualization of the rate of change in emitted fluorescence during temperature change. A derivative melt curve from PCR fragments without mutations will give rise to one distinct peak, representing the sequence specific melting point. A change in the sequence will alter the slope and the melting point, indicating a mutation in the gDNA.

Genomic DNA was extracted, when the animals reached primary polyp stage, from the injected animals and the wildtype (WT) control animals. Animals were subjected to 5 min

incubation in 100% EtOH, before letting the animals dry at 50°C for 45 min. Genomic extraction buffer was added to the animals before a 2 h incubation at 50°C followed by 10 min incubation at 98°C. A PCR reaction was performed on a approx. 100 bp amplicon spanning the sgRNA cut site, by preparing a 30 µl reaction containing 6 µl 5X Q5 buffer, 0.75 µl dNTPs (10mM), 1 µl fwd and rev primer (10 mM) (Table 2.7), 0.25 µl Q5 High-Fidelity DNA Polymerase (2.5 U/µl), 1.5 µl 20X EvaGreen® Dye and 2 µl genomic DNA from each extraction, both injected and WT gDNA. The PCR program contained one round of 3 min initial denaturation at 98°C, 40 cycles of 30s at 98°C, 30s at 60°C and 5s at 72°C, ending with a 3 min final extension at 72°C. The PCR product was then analyzed by C1000 Thermal Cycler (BioRad) with the following program: starting temperature at 60°C, followed by a 0.5°C incremental increase in temperature while the fluorescence is measured until the temperature reached 95°C.

4 Results

This thesis aimed to investigate the expression of components of the DGC and of glycosyltransferases participating in *O*-linked mannosylation in *Nematostella*. As *POMGNT1* has previously been found to be upregulated in the *FoxQ2d*-expressing sensory cell population, it was selected for the generation of CRISPR/Cas9-induced mutations for future functional analyses.

4.1 Expression pattern of the glycosyltransferases responsible for α-DG glycosylation

In situ hybridization was performed to detect the presence and specific localization of the transcripts for the glycosyltransferases functioning in *O*-linked mannosylation in *Nematostella*. The aim was to detect if and where the transcripts for the enzymes *POMGNT1, POMGNT2, POMT1, POMT2* and *fukutin* are present during the early development of *Nematostella*.

4.1.1 *POMGNT1* is expressed in scattered cells during the early stages, with a more tissue specific pattern in later stages

POMGNT1 is present in a scattered pattern with single cells in the ectoderm (outer) layer through gastrula (20 hours post fertilization, [hpf]) (Figure 4.1 A-D) and late gastrula (30 hpf) stages (Figure 4.1 E-H). The expression is restricted to the more aboral part of the embryo. In the early planula (48 hpf), the expression displays a stained area in the aboral-most part of the ectoderm and some staining in the mesendoderm (Figure 4.1 I-L). Some dark round spots are present in the mesendoderm at early planula stage, but such spots are also visible in a control with a sense probe at the early planula stage (Figure 4.1 I-P, black arrow). These spots are therefore believed to be unspecific accumulation of staining (Figure 4.1 I-P, black arrow). Planula stage (72 hpf) shows a further concentration of *POMGNT1*-expressing cells at the aboral pole (Figure 4.1 Q-R, orange arrow) and in the mesendoderm of the embryo. There is some expression in individual cells in the ectoderm along the body and in the region close to the oral opening in planula stage (Figure 4.1 Q-R, green arrows). The apical pole staining is not as prominent in the late planula (96 hpf) but there is still some weak staining clustered to the apical pole (Figure 4.1 S-T, orange arrow), in addition to a uniform staining throughout

the mesendoderm with some darker areas extending along the oral-aboral axis likely corresponding to the forming mesenteries. The expression of *POMGNT1* is uniform in the mesendoderm, pharyngeal ectoderm (Figure 4.1 U, yellow arrow), the forming mesenteries (Figure 4.1 U, blue arrows), and the tentacles in primary polyp stage (6 dpf) (Figure 4.1 U-V). Taken together, the expression of *POMGNT1* is observed from gastrulation to primary polyp. The pattern is observed as scattered cells in the ectoderm, and in the mesendoderm at later stages.

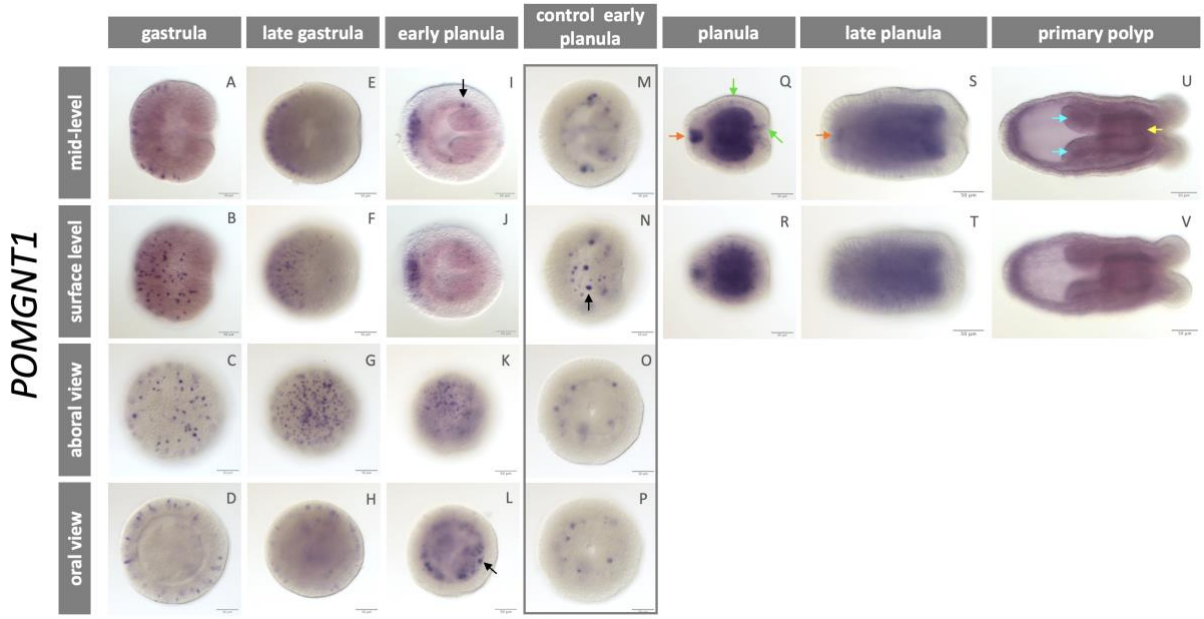

Figure 4.1: Expression pattern of *POMGNT1* in *Nematostella vectensis.* (A-V) *In situ* hybridization of *POMGNT1* was performed on six developmental stages in *Nematostella vectensis*. The stages are indicated on the top and the different focal planes or views on the left side. The orientation of the embryo is always with the oral pole to the right and aboral pole to the left. At gastrula stage (20 hpf) and throughout late gastrula stage (30 hpf), *POMGNT1* is expressed as scattered cells in the ectoderm layer clustered towards the aboral pole **(A-H).** The expression becomes denser in the aboral pole at early planula stage (48 hpf) **(I-L)**. At this stage, there are dark spots of unspecific staining present (black arrows), confirmed with a sense control probe for this stage (indicated with a box) **(M-P)**. Planula stage (72 hpf) displays a dense accumulation of expression in the apical organ (orange arrow), in the mesendoderm, a few scattered cells in the ectoderm and at the oral opening (green arrow) **(Q-R)**. The apical organ displays a weak expression in the late planula (96 hpf) (orange arrow), in addition to a uniformly stained mesendodermal area with primary mesenteries **(S-T)**. Primary polyp stage (6 dpf) shows expression in the mesendodermal mesenteries, pharynx and mesendodermal tentacles **(U-V)**. The scale bar represents 50 μm.

4.1.2 *POMT1* and *POMT2* display similar expression patterns during early development

The expression patterns of *POMT1* and *POMT2* show resemblance to each other especially at the early stages. Gastrula and late gastrula stage show scattered cells in the ectoderm for both genes, where the expressing cells are largely restricted to the aboral part of the embryo (Figure 4.2 A-H, and Figure 4.3 A-H). Some cells expressing these genes are also seen in more oral parts of the ectoderm, more prominently for *POMT2* (Figure 4.2 A-H, and Figure 4.3 A-H). The early expression pattern in gastrula and late gastrula of *POMT1* and *POMT2* resembles the expression pattern of *POMGNT1* in the same stages. At early planula stage, *POMT1* is expressed in scattered cells throughout the ectoderm (Figure 4.2 I-L), whereas at the same stage *POMT2*-expressing cells are mainly found close to the aboral pole (Figure 4.3 I-L). As for *POMGNT1*, a sense probe control for early planula shows the unspecific round spots at this stage (Figure 4.2 M-N and 4.3 M-N). *POMT1* expression in planula and late planula is mostly found in the mesendoderm, with a few cells in the ectoderm, and an ectodermal accumulation at the oral end where the tentacle buds will form (Figure 4.2 O-R, black arrows). Expression of *POMT2* at the planula stage shows some staining in the ectoderm but most uniformly in the mesendoderm, with a weak indication of staining where the tentacles will develop at the oral pole (Figure 4.3 O-P). At the late planula stage, *POMT2 expression* is also present in the developing tentacle buds (Figure 4.3 Q-R, black arrows). Both *POMT1* and *POMT2* are expressed similarly at primary polyp stage, with a uniform staining in the mesendoderm, the ectodermal pharynx, the mesenteries, and some weak staining in the mesendodermal tentacles (Figure 4.2 S-T and Figure 4.3 S-T, green arrows). Thus, the expression patterns of *POMT1* and *POMT2* are mostly similar throughout the development of *Nematostella* from gastrula to primary polyp, with an early expression in scattered ectodermal cells and later expression in the mesendoderm and the tentacle buds.

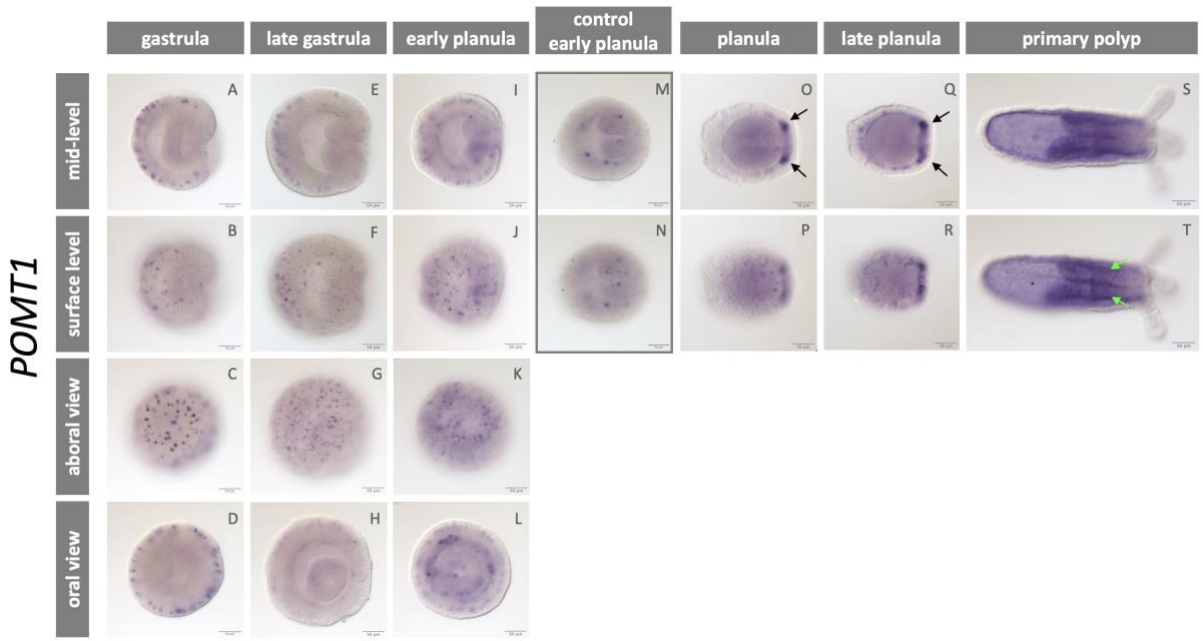

Figure 4.2: *POMT1* expression pattern by *in situ* hybridization. (A-T) Embryos from different developmental stages were subjected to *in situ* hybridization to detect the localization of *POMT1*. The stages are indicated on the top of the figure, while the different focal planes or views are indicated on the left side. The embryos are oriented with the oral pole to the right and aboral pole to the left. At gastrula (20 hpf) and late gastrula stage (30 hpf), *POMT1* is expressed in scattered cells in the ectoderm layer clustered towards the aboral pole **(A-H)**. At early planula stage (48 hpf) single cells are scattered more evenly throughout the ectoderm **(I-L)**. The dark spots of staining present at this stage, are unspecific staining confirmed with a sense control (indicated with a box) **(M-N)**. Planula stage (72 hpf) and late planula stage (96 hpf) show staining mostly in the mesendoderm, with some staining in the ectoderm and accumulation of stained cells in the tentacle buds (black arrows) **(O-R)**. Expression at the primary polyp stage (6 dpf) is found in the mesenteries (green arrows) and the pharynx **(S-T)**. The scale bar represents 50 μm.

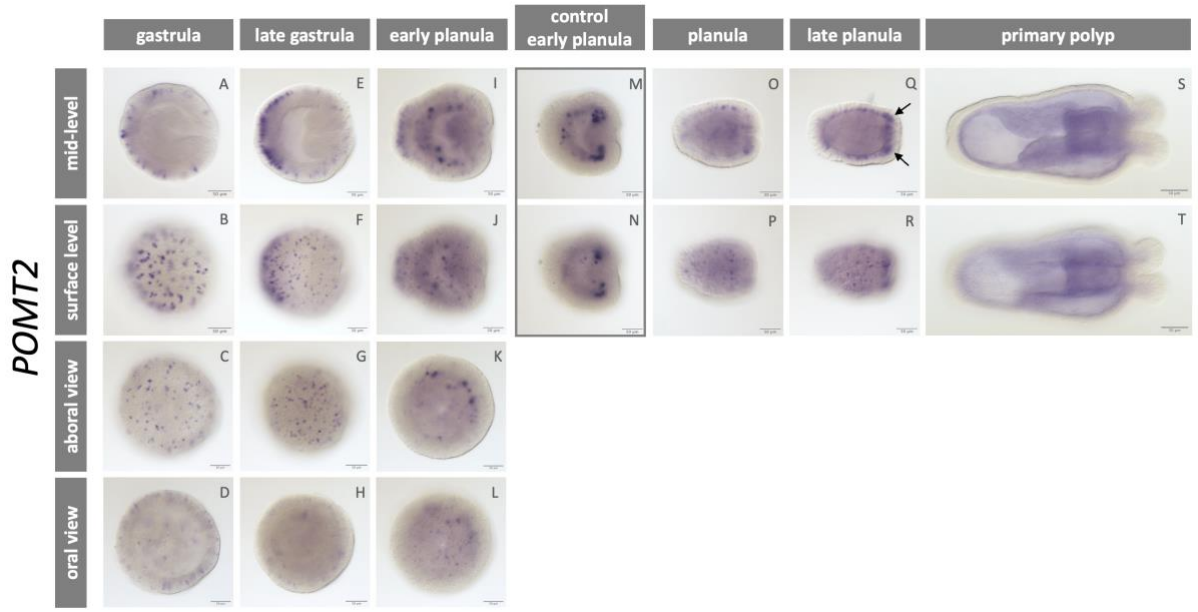

Figure 4.3: *POMT2* expression pattern resembles expression of *POMT1.* (A-T) *In situ* hybridization was performed on *Nematostella* embryos from different developmental stages to detect the localization of *POMT1*. The stages are indicated on the top, while the focal planes or views are indicated vertically on the left side of the

figure. The animals are oriented with the oral pole to the right. At gastrula stage (20 hpf) and late gastrula stage (30 hpf), *POMT2* shows an expression pattern resembling that of *POMT1*, with scattered cells accumulated towards the aboral pole in the ectoderm layer **(A-H)**. At early planula stage (48 hpf) there are still clustered cells in the ectoderm at the aboral pole, with mesendodermal expression and presence of stained spots in the mesendoderm **(I-L)** confirmed to be unspecific with a sense probe control (indicated with a box) **(M-N)**. The expression of *POMT2* shows high similarity to *POMT1* at planula (72 hpf) and late planula stage (96 hpf). In these stages the expression is broadly mesendodermal, and in some ectodermal cells in addition to a more intense staining at the oral pole where the tentacles will form (black arrows) **(O-R)**. Expression in the primary polyp stage (6 dpf) is as for *POMT1* and *POMGNT1*, found in the mesendodermal mesenteries, and the pharynx **(S-T)**. Scale bar: 50 μm.

4.1.3 *POMGNT2* is more prominently expressed at later stages of development

The gastrula stage indicates specific staining of *POMGNT2* in a low number of scattered cells throughout the ectoderm (Figure 4.4 A-D). A few mesendodermal cells expressing *POMGNT2* are visible at late gastrula stage (Figure 4.4 E-H). Early planula displays areas with expression in the mesendoderm in addition to the unspecific spots of staining (Figure 4.4 I-L). The aboral and oral view of the early planula sense control, also display expression in the mesendoderm, suggesting that this staining is unspecific (Figure 4.4 M-P). In contrast, the planula and late planula stage shows uniform mesendodermal expression of *POMGNT2* (Figure 4.4 Q-T). At primary polyp stage, the mesendodermal tissue, the pharynx, and the mesenteries also show uniform expression of *POMGNT2* (Figure 4.4 U-V, orange arrows). In the developing tentacle buds, the mesendodermal tissue is showing expression of *POMGNT2* (Figure 4.4 U-V). From late gastrula stage to primary polyp, the ectoderm layer shows no visible expression. The expression of *POMGNT2* differs from the other enzymes, with less expression in early stages, but indicates the same mesendodermal expression at primary poly stage.

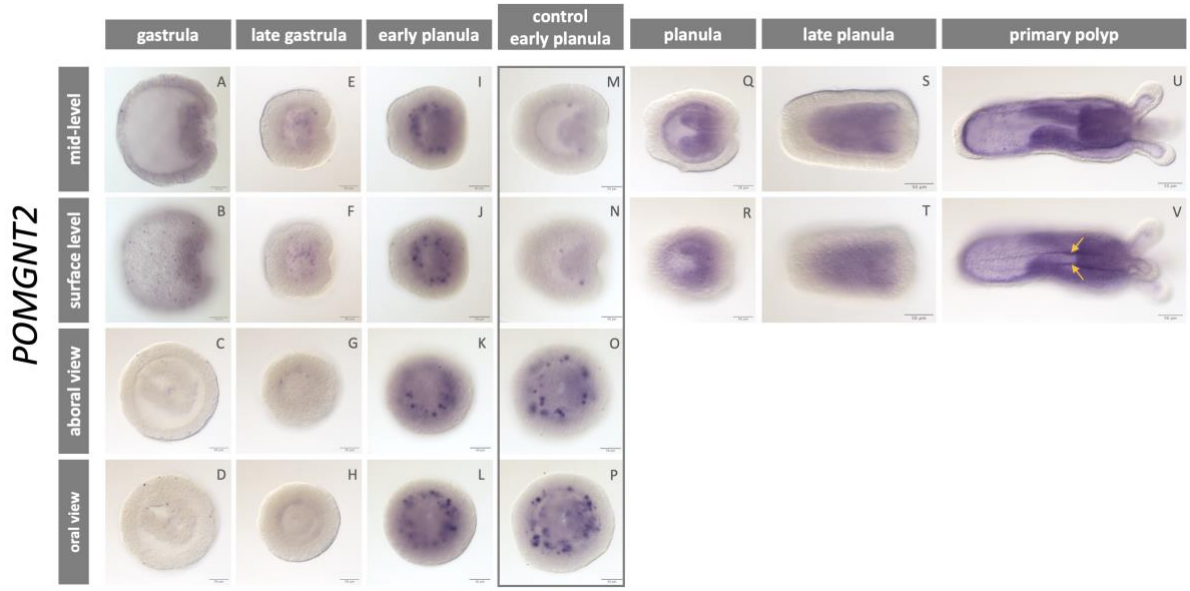

Figure 4.4*: Expression pattern of POMGNT2 in Nematostella vectensis.* **(A-V)** *In situ* hybridization was performed on embryos from different developmental stages to detect the localization of *POMGNT2* expression. The orientation of the animals is with the oral pole to the right and aboral pole to the left. The developmental stages are indicated at the top of the figure, with the focal planes and views indicated on the left. The expression is low at gastrula stage (20 hpf) with a scattered cells present in the ectoderm **(A-D).** At late gastrula stage (30 hpf), *POMGNT2* expression is found in the mesendoderm **(E-H)**. At early planula stage (48 hpf) there are some darker stained areas in the mesendoderm with the unspecific dark spots **(I-L)**, as the staining pattern in the control (indicated with a box) **(M-P)**. Mesendodermal expression of *POMGNT2* is present at planula (72 hpf) and late planula stage (96 hpf) **(Q-T)**. The primary polyp (6 dpf) is expressing the gene in the mesenteries (orange arrows), and the pharynx but also the mesendodermal tissue of the tentacles **(U-V)**. Scale bar: 50 μm.

4.1.4 *Fukutin* is expressed early in scattered cells and in the mesendoderm at later stages

At gastrula stage the expression of *fukutin* is distributed as a scattered pattern of single cells throughout the ectodermal layer of the embryo (Figure 4.5 A-D), resembling the expression of the other glycosyltransferases. The expression is decreased at late gastrula stage with a few scattered ectodermal cells, in addition to a stained area in the mesendoderm. At the blastopore there is a change of staining intensity to lower levels in the body wall ectoderm (Figure 4.5 E-F, black arrows). Early planula stage shows expression of *fukutin* in the mesendoderm layer with staining in the developing pharynx at the oral pole (Figure 4.5 I-L, black arrows). This stage has the presence of the round dark spots believed to be unspecific staining because of the similar spots present in the sense control animals (Figure 4.5 M-P). A few *fukutin*-expressing cells can be observed in the ectoderm layer at planula stage (Figure 4.5 R), with the addition of uniform staining in the mesendoderm (Figure 4.5 Q-R). At late planula the embryo shows the same expression in the mesendoderm, with a few *fukutin*-expressing cells in the ectoderm (Figure 4.5 S-T, orange arrows). At the primary polyp stage,

fukutin is expressed in a pattern resembling the other genes, with staining throughout the mesendodermal tissue, the mesenteries, and the pharynx (Figure 4.5 U-V).

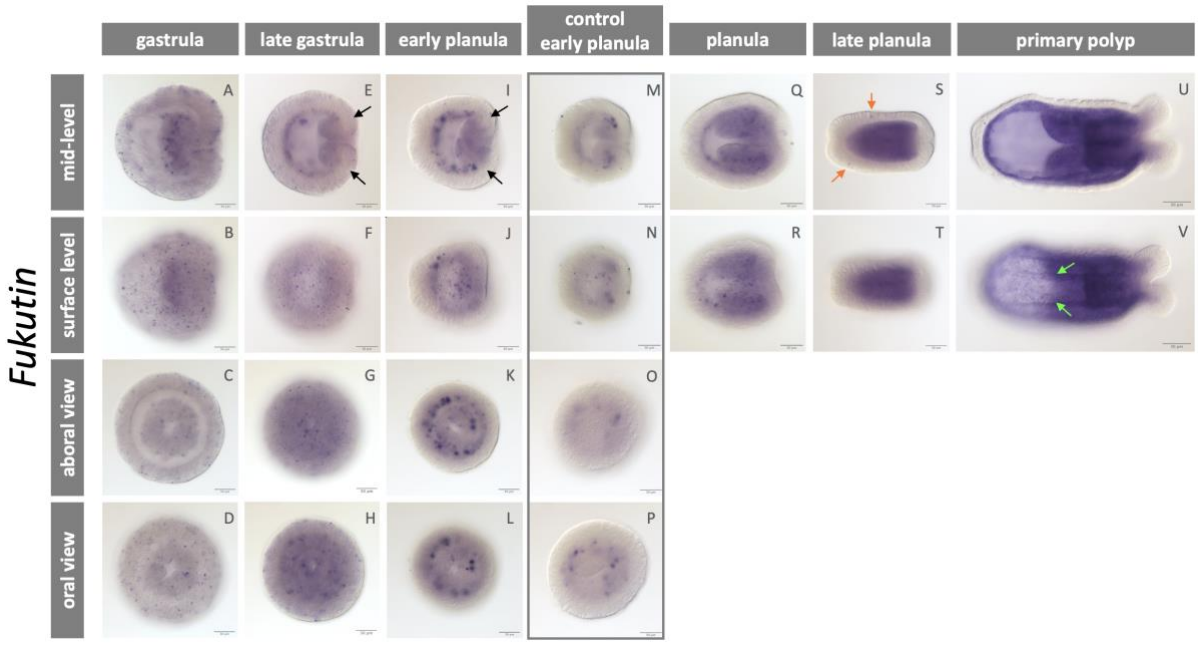

Figure 4.5*: Expression pattern of fukutin develops from being ectodermal to mostly mesendodermal.* (A-V) By performing *in situ* hybridization, the expression pattern of *fukutin*-expressing cells was detected in embryos from different developmental stages. The oral pole of the animal is oriented to the right. The developmental stages are indicated at the top, while the different focal planes and views are indicated vertically on the left side. *Fukutin*-expressing cells are located in the ectoderm and mesendoderm at gastrula stage (20 hpf) **(A-D)**. At late gastrula stage (30 hpf), the amount of expressing cells is slightly reduced **(E-H)**. At early planula stage (48 hpf) the unspecific dark spots are present in addition to some darker stained areas in the mesendoderm **(I-L)**. The early planula sense control has the same unspecific spots (indicated with a box) **(M-P)**. Mesendodermal and ectodermal expression of *fukutin* is present at planula (72 hpf) and late planula stage (96 hpf) (**Q-T**, orange arrows). The mesenteries, the pharynx and the mesendodermal tissue in the tentacles expresses *fukutin* at primary polyp stage (6 dpf) **(U-V)**. Scale bar represents 50 μm.

4.2 Detection of *dystroglycan* and *dystrobrevin* as part of the DGC in *Nematostella vectensis*

ISH was performed to detect the presence and localization of the *dystroglycan* and *dystrobrevin* transcripts within *Nematostella*. These proteins are a central part of the DGC in bilaterians.

In the gastrula, expression of *dystrobrevin* was detected only in a few single cells in the ectoderm (Figure 4.6 A-D, orange arrows). There is an increase in the number of single cells expressing *dystrobrevin* in late gastrula, with the aboral view indicating cells present in both ectoderm and mesendoderm tissue (Figure 4.6 E-H). The staining in early planula is restricted

to the mesendodermal part of the embryo, with the presence of some round, dark spots (Figure 4.6 I-L, black arrows), concluded to be unspecific as they are also present in the early planula control animals (Figure 4.6 M-P, black arrows). At planula and late planula stages, expression was not detectable in the ectoderm, but uniformly in the mesendoderm, with the primary mesenteries more intensely stained (Figure 4.6 Q-T, green arrows). The expression of *dystrobrevin* is still restricted to the mesendoderm at primary polyp stage, where the pharynx, mesenteries and the mesendodermal part of the tentacles display expression.

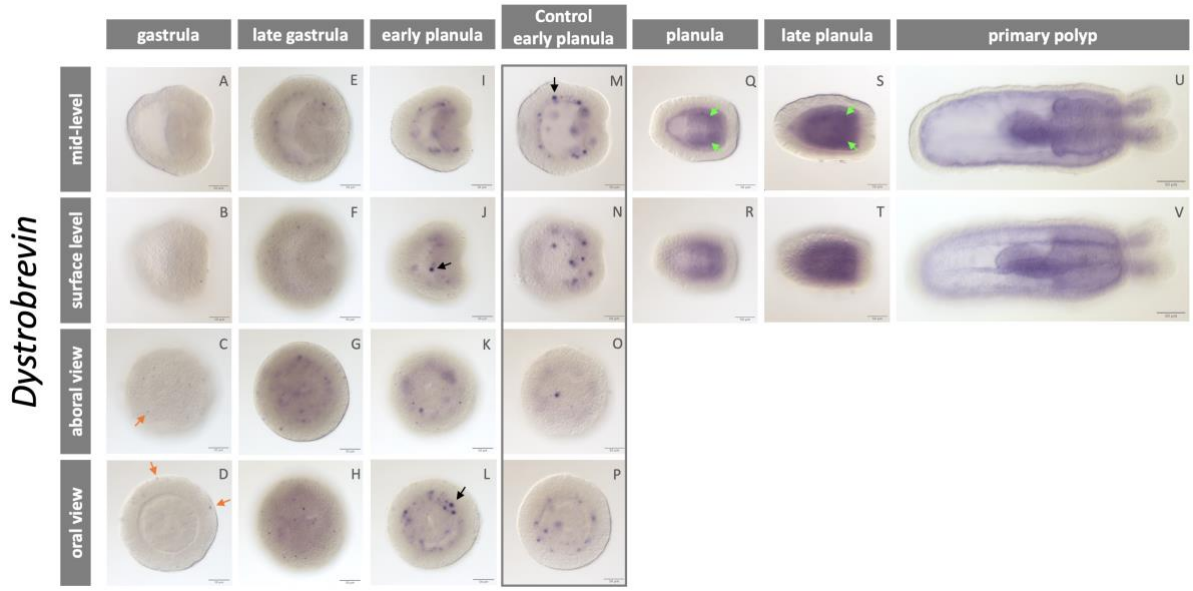

Figure 4.6*: Dystrobrevin is mostly expressed in later stages of development.* The expression pattern of *dystrobrevin* was investigated by means of *in situ* hybridization. The developmental stages are indicated on the top of the figure, while the different focal plane and views indicated to the left. The animals are orientated with the oral pole towards the right and aboral pole towards the left. At gastrula stage (20 hpf) there are only a few scattered cells present in the ectoderm (**A-D**, orange arrows). At late gastrula stage (30 hpf), the expression is a bit stronger with a few cells in the ectoderm and some mesendodermal staining (E-H). Early planula stage (48 hpf) contains the unspecific dark spots (**I-L**, black arrows), as do the controls (indicated with a box) **(M-P)**. Expression of *dystrobrevin* is present in planula (72 hpf) and late planula stage (96 hpf) within the mesendoderm and at higher levels in the formin mesenteries (**Q-T**, green arrows). The primary polyp is expressing the gene in the mesenteries, the pharynx and in addition the mesendodermal tentacles **(U-V)**. Scale bar: 50 μm.

In contrast to *dystrobrevin*, the expression of *dystroglycan* is present in a higher number of single cells distributed throughout the whole ectoderm of the gastrula stage embryo (Figure 4.7 A-B). Late gastrula stage is exhibiting a clearly stained mesendoderm with some expression around the oral opening at the blastopore (Figure 4.7 E-H, orange arrows). Early planula stage shows the same expression pattern as late gastrula stage, with mesendodermal expression and some indication of staining at the oral opening (Figure 4.7 I-L, orange arrows). The sense control animals display the unspecific spots of staining which are also present in

the early planula stage animals hybridized with the antisense probe (Figure 4.7 M-P). The expression pattern is maintained in the mesendodermal part of the animal at planula stage and late planula stage. The staining is more intense in the developing mesenteries in both stages (Figure 4.7 Q-T, yellow arrows). In primary polyp, the expression of *dystroglycan* resembles the expression of the other genes with a staining in the mesenteries, as well as the mesendodermal layer of the tentacles (Figure 4.7 U-V, green arrows).

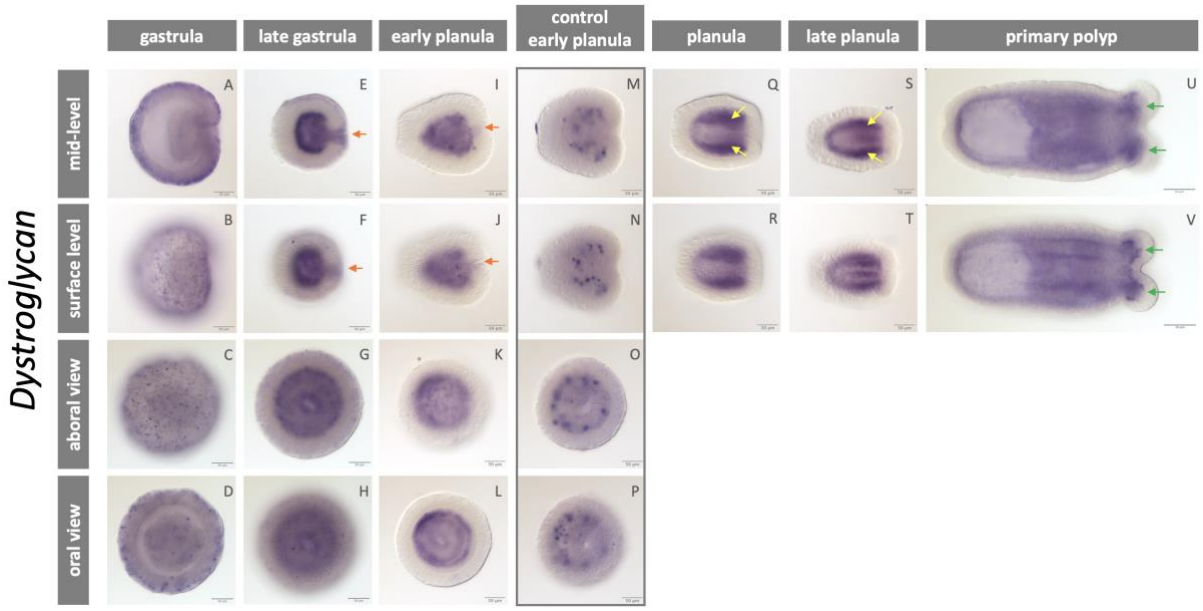

Figure 4.7*: Dystroglycan is mostly expressed in the mesendoderm throughout the development of Nematostella vectensis.* (A-V) The expression of *dystroglycan* in *Nematostella* in different developmental stages, was studied by *in situ* hybridization. The stages and the different views are indicated at the top, and on the side of the figure. The orientation of the embryo is always placed with the oral pole to the right. From gastrula stage (20 hpf) to late gastrula stage (30 hpf), the expression pattern changes from scattered cells in the ectoderm to be more expressed in the mesendoderm and at the blastopore (**A-H,** orange arrows). At early planula stage (48 hpf) the expression in still mesendodermal, with a weak detection at the blastopore (**I-L**, orange arrows). Early planula control animals show the unspecific spots of staining at this stage (indicated with a box) **(M-P)**. Expression of *dystroglycan* is strongly present in the mesendoderm, and the developing mesenteries at planula (72 hpf) and late planula stage (96 hpf) **(Q-T)**. Primary polyp stage (6 dpf) shows expression in the pharynx, the mesenteries and the mesendodermal tissue of the tentacles **(U-V)**. The scale bar indicates 50 μm.

To summarize the colorimetric ISH results, the enzymes responsible for the *O*-mannosylation of α-DG display a similar expression pattern in the early stages with scattered cells in the ectoderm. Especially for *POMGNT1*, *POMT1* and *POMT2* there is a higher density of labelled cells at the aboral end of the embryo. For the later stages, especially in primary polyp, expression is present in the whole mesendoderm, and more intensely in the mesenteries and

pharynx. As for *dystroglycan* and *dystrobrevin*, the expression pattern at later development is similar to the enzymes with broad mesendodermal and pharyngeal staining.

4.3 Co-expression of glycosyltransferases detected by double fluorescence *in situ* hybridization

To further investigate the expression patterns of the glycosyltransferases in *Nematostella*, double fluorescence *in situ* hybridization (dFISH) was performed. This revealed partial co-expression of some of the transferases, and co-expression between *POMGNT1* and *FoxQ2d*, a gene expressed in the nervous system.

4.3.1 Co-expression was observed between *POMT1* and *POMT2*

The glycosyltransferases responsible for the second step in the glycosylation of α-DG, *POMT1* and *POMT2* showed comparable expression patterns in the colorimetric *in situ* hybridizations in *Nematostella*. As the two enzymes have been found to co-localize in other species, they were therefore subjected to dFISH to investigate possible co-expression in *Nematostella* embryos. *POMT1* was found to be co-expressed with *POMT2* in scattered cells at the ectodermal aboral end at gastrula stage (Figure 4.8 A). The white arrow indicates some unspecific signal at gastrula stage (Figure 4.8 A, white arrow). Late gastrula stage displays an embryo from the aboral view, where the majority of cells expressing *POMT2*, are also expressing *POMT1* in a scattered pattern in the ectodermal layer (Figure 4.8 B). At late gastrula, some cells seem to only express *POMT2*, while cells expressing only *POMT1* were not detected (Figure 4.8 B, arrows in cyan).

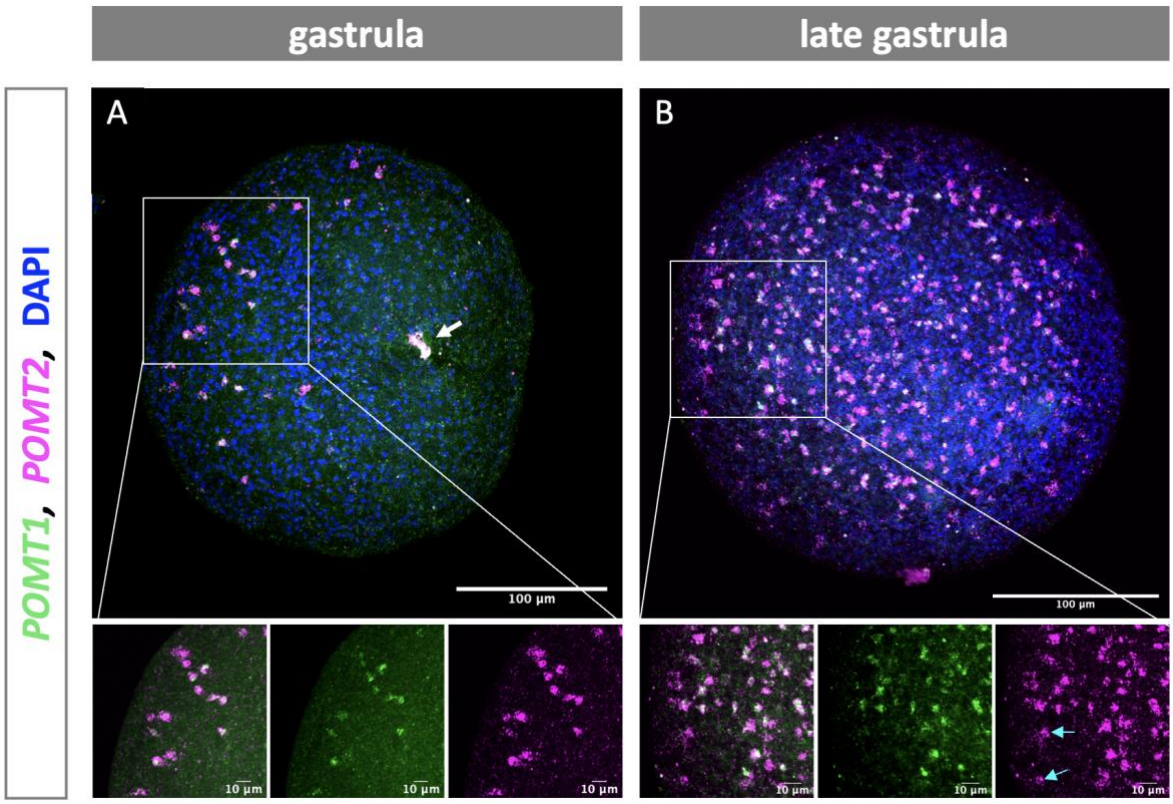

Figure 4.8*:* Co-expression of *POMT1* and *POMT2* at gastrula stages. **(A-B)** Embryos from gastrula (20 hpf) and late gastrula (30 hpf) stage were subjected to dFISH to detect the potential co-expression of *POMT1* (green) and *POMT2* (magenta). The gastrula stage embryo **(A)** is oriented with the oral pole to the right, while late gastrula stage **(B)** is oriented as an aboral view. The white boxes indicate the location of the close-up image. *POMT1* is co-expressed with *POMT2* in a scattered pattern at the ectodermal aboral pole at gastrula stage **(A)**. Unspecific staining is marked with a white arrow **(A)**. Late gastrula stage also shows co-expression of *POMT1* and *POMT2* from an aboral view **(B)**. In this stage, there are some cells only expressing *POMT2* (**B**, arrows in cyan). The scale bars represent 100 µm (overview images) and 10 µm (close-up images at the bottom).

4.3.2 Partial co-expression of *POMGNT1* with *POMT1* and *POMT2*

The colorimetric ISH indicated *POMGNT1* to have a similar expression pattern as *POMT1* and *POMT2* in the early stages of *Nematostella* development. Therefore, dFISH was performed to investigate if *POMGNT1* is co-expressed with *POMT1* and *POMT2* in late gastrula stage. The majority of *POMT1* expressing cells were found to also express *POMGNT1* in a scattered pattern in the ectoderm layer (Figure 4.9 A). Similar results were observed for *POMGNT1* and *POMT2* where co-expressing cells were found in the ectodermal aboral part of the embryo (Figure 4.9 B). However, for both *POMT1* and *POMT2*, the co-expression is not absolute as there are cells only expressing *POMGNT1.* In the co-expression of *POMGNT1* and *POMT2*, there is some unspecific staining present at the edge of the embryo (Figure 4.9 B, white arrow) The arrows in cyan shows examples of co-expressing cells (Figure 4.9 A-B).

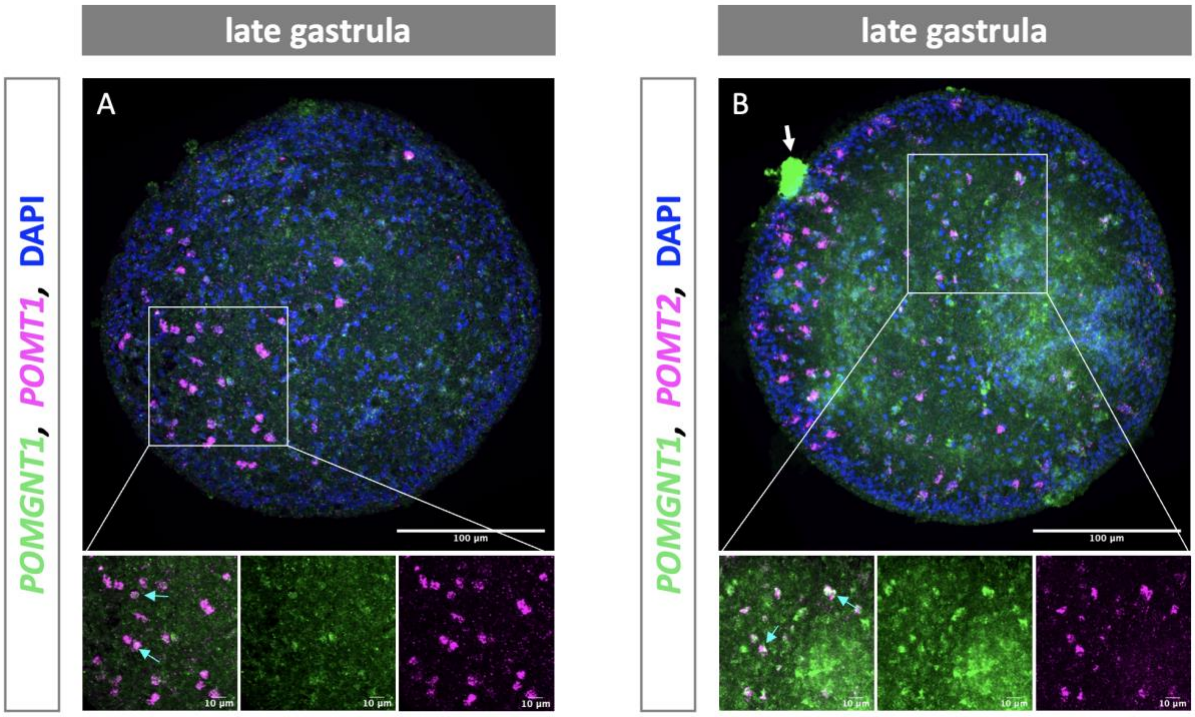

Figure 4.9*: POMT1* and *POMT2* are both co-expressing with *POMGNT1*. (A-B) dFISH was performed on embryos at late gastrula (30 hpf) stage to detect if any co-expression was present between *POMGNT1* and *POMT1* and *POMGNT1* and *POMT2*. Both embryos are oriented with the oral pole to the right and aboral pole to the left **(A-B)**. The white boxes indicate the location of the close-up image. *POMGNT1* is found to be partially co-expressed with *POMT1* and *POMT2* in a scattered pattern at the ectodermal aboral pole at gastrula stage (**A-B**, cyan arrows indicating example of co-expression) Unspecific staining is marked with a white arrow **(B)**. The scale bars represent 100 µm (overview images) and 10 µm (close-up images at the bottom).

4.3.3 *POMGNT1* co-expressed with some *NvFoxQ2d* expressing cells

Considering that *POMGNT1* is found in the transcriptome of *FoxQ2d*::mOrange-expressing cells, it was interesting to investigate a potential co-expression. dFISH did show co-expression between *POMGNT1* and *FoxQ2d* in one elongated cell present in the ectoderm of *Nematostella* embryo at gastrula stage (Figure 4.10). In addition, some cells with a round morphology are expressing *POMGNT1* and *FoxQ2d*. Some of the small, scattered spots throughout the embryo do not conform with the typical *in situ* hybridization signal and are therefore believed to be unspecific signal.

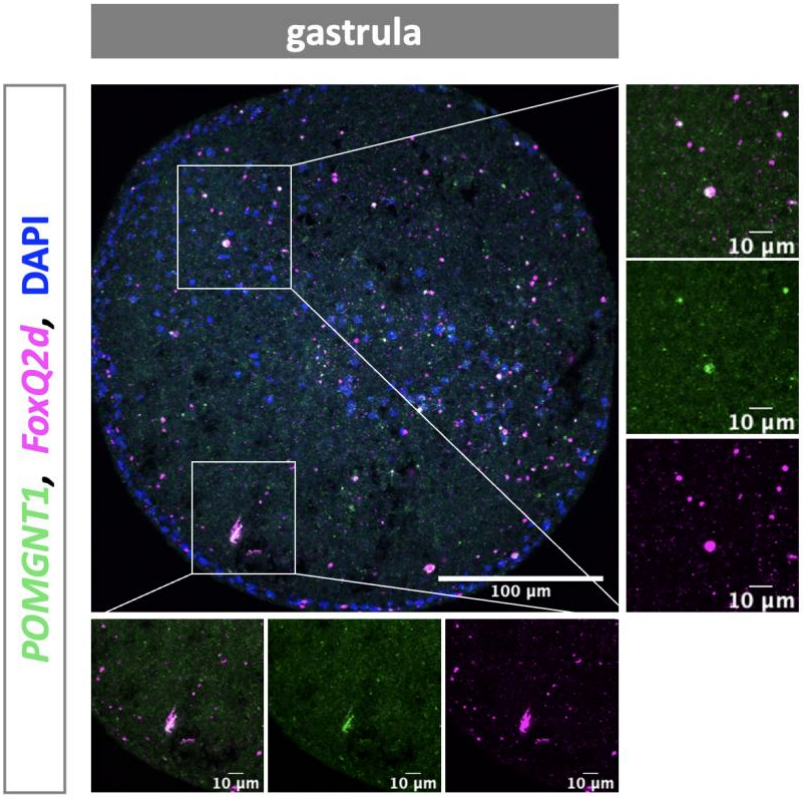

Figure 4.10: *FoxQ2d*-expresing cells also express *POMGNT1*. dFISH showing expression of *FoxQ2d* and *POMGNT1* at gastrula stage (20 hpf). The orientation of the embryo is with the oral pole to the right and aboral pole to the left. The white box indicates the location of the close-up image. *POMGNT1* is found to be co-expressed with at least one *FoxQ2d*-expressing cell at the ectodermal layer. The scale bars represent 100 µm (overview), and 10 µm for the close-up images.

4.4 Successful generation of *POMGNT1* F0 mutants by CRISPR/Cas9 genome editing

After determining the expression patterns of the glycosyltransferases, we aimed at obtaining insight into the function of these genes in *Nematostella.* We focused on *POMGNT1* because of its upregulation in *FoxQ2d*::mOrange positive cells, which indicates a possible role in nervous system development. Genome editing by the CRISPR/Cas9 system was used to introduce a mutation in the *POMGNT1* gene. *POMGNT1* has a size of 4336 bp with 6 coding exons. A guide RNA (gRNA) was designed to target the beginning of the second coding exon consisting of 269 bp, with the goal to induce an indel mutation that creates a frameshift (Table 2.7) (Figure 4.11).

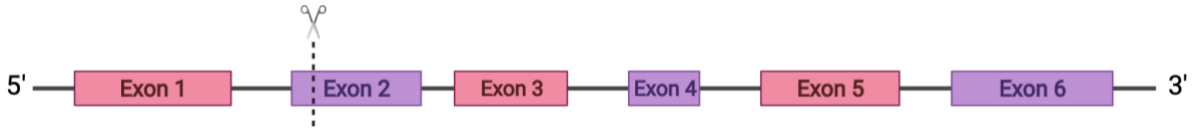

Figure 4.11*: Illustration of POMGNT1* and the targeting strategy of CRISPR/Cas9. *POMGNT1* has a size of 4336 bp, with six coding exons. Exon number 2, consisting of 269 bp, and is being targeted to induce a mutation by CRISPR/Cas9 genome editing method. The dotted line indicates the cut site. The figure is not to scale.

Fertilized *Nematostella* eggs were injected with the sgRNA and Cas9 protein and grown to primary polyp stage before genomic DNA (gDNA) was extracted from eight injected and eight WT animals. PCR fragments of the targeted region were then analyzed with EvaGreen® melt curves to verify the presence of a mutation. In the absence of mutations, a single peak is observed in the melt curve. The introduction of a mutation is visible as a change in the slope of the melt curve or by the appearance of a second peak.

A representative for the WT control is shown in blue, while injected animals are shown in magenta (Figure 4.12). The majority of the injected animals displays a shift in the derivative slope, compared to the control animals (Figure 4.12 A). 4/8 slopes of the PCR fragments from injected animals display a “shoulder” at a lower temperature, therefore have a lower melting point than the control fragments. These alterations of the slopes indicate a change in the sequence, and therefore a mutation in the DNA sequence. The figure includes examples of a WT curve compared to one successfully generated mutant (Figure 4.12 B) and one that did not show any shift in the melt curve and are concluded to not contain a mutation in the sequence (Figure 4.12 C). The wild-type peak is still present in mutant F0 animals due to the mosaicism of the introduced mutation. We conclude that the CRISPR/Cas9 approach can create mutations in *POMGNT1*, but the exact nature of the mutation cannot be concluded from the melt curve alone.

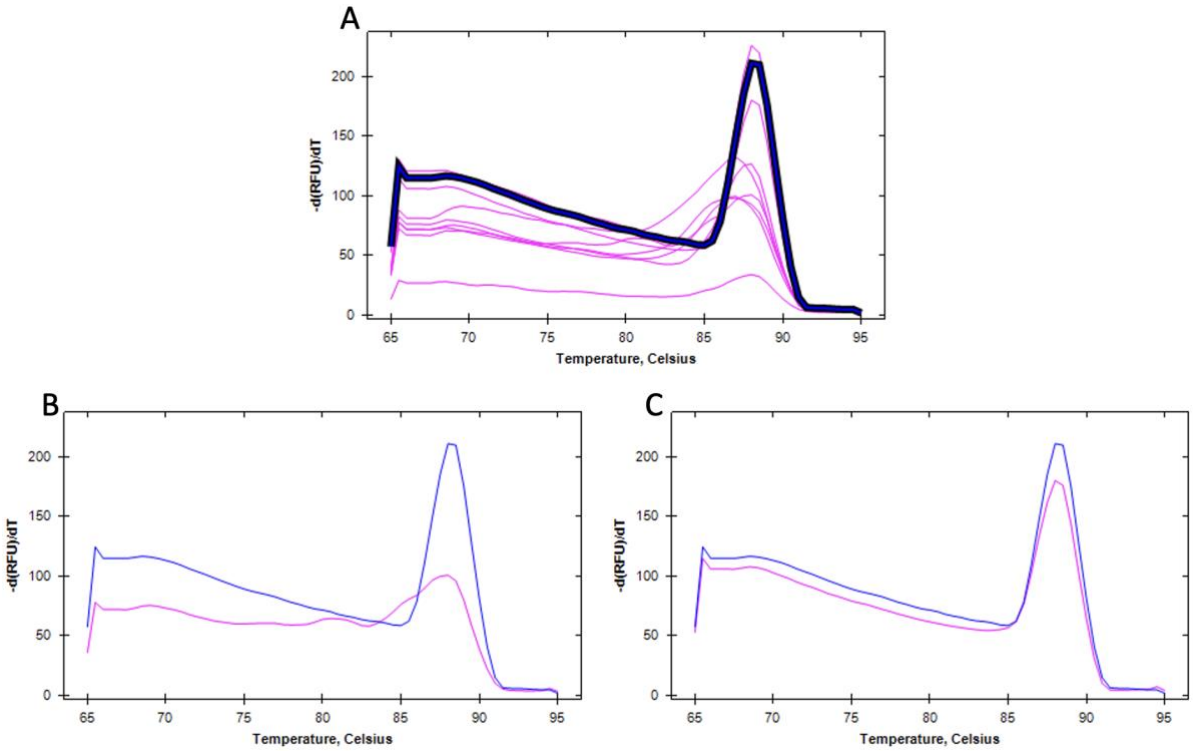

Figure 4.12: Melt curves representing mutations induced in *POMGNT1* injected animals. (A-C) *Nematostella vectensis* zygotes were injected with sgRNA to induce a mutation in *POMGNT1*, grown to primary polyp stage when gDNA of eight injected and eight WT animals was extracted and analyzed by EvaGreen melt curve. Alternated DNA will cause a change in the slope compared to the control. The control WT gDNA is shown in blue, while the eight injected animals are shown in magenta **(A)**. One successful mutation is shown compared to the control slope in **(B)** and the slope of one injected animal concluded to not be mutant is compared to WT in **(C)**. 4/8 animals show a shift and the presence of a "shoulder" in the melting curve compared to the control, which indicates a successful mutation in the sequence of *POMGNT1.* The x-axis represents the temperature in °C, while the Y-axis show the change of fluorescence per unit change in temperature [-d(RFU)/dT].

The surviving injected animals were raised and will start spawning when reaching sexual maturity. Then, the injected F0 animals can be crossed with WT animals, where sequencing of the DNA of tissue pieces will confirm possible mutation in F1 animals. If a mutation is present, the F1 animals will be used to obtain homozygous mutants.

5 Discussion

O-mannosyl glycosylation of α-dystroglycan (α-DG) plays an important role in the development and physiology of the nervous system and the musculature in vertebrates and other bilaterians (Wells, 2013). Here we analyzed the expression patterns of α-DG and glycosyltransferases in the cnidarian *Nematostella vectensis* and show that these expression patterns are compatible with α-DG-dependent and -independent roles of *O*-mannosylation. Further, animals with a mutation in the *POMGNT1* gene were successfully generated by CRISPR/Cas9.

5.1 Expression patterns of glycosyltransferases support cell type specific roles of *O*-mannosylation in *Nematostella*

Colorimetric ISH revealed similar expression patterns for the *O*-mannosylation-related glycosyltransferases (Figure 4.1-4.5). At gastrula and late gastrula stage, they display an interesting expression pattern with single cells scattered in the ectoderm. This is especially prominent for *POMGNT1, POMT1* and *POMT2*, where the expressed cells accumulate at the aboral region of the embryo. dFISH confirmed co-expression of *POMT1* and *POMT2* at both gastrula and late gastrula stage. Similar results were observed for *POMT2* and *POMGNT1*, where a partial overlap was present. *POMT1* and *POMT2* are believed to form an enzymatic heterodimer within the endoplasmic reticulum, where they both are needed for enzyme activity (Bigotti and Brancaccio, 2021). Studies performed on mammalian cells, have shown that co-expression of *POMT1* and *POMT2* is necessary for the enzyme activity, while expression of either of them alone was proven to be insufficient (Manya et al., 2004). The co-expression of *POMT1* and *POMT2*, and the similarity with the expression patterns of *POMGNT1* and *fukutin* support a scenario in which these enzymes function together to generate complex *O*-mannosylation patterns. The expression patterns indicate that at early stages such *O*-mannosylation patterns are particularly important in specific cells in the ectoderm.

5.2 A potential role for *O*-mannosylation of α-Dystroglycan in later stages of development

ISH revealed that the glycosyltransferases *POMGNT1, POMGNT2, POMT1, POMT2* and *fukutin* all show a similar expression pattern in later stages, with staining throughout the mesendoderm. This expression pattern is also very similar to that of *dystroglycan* and *dystrobrevin* (Figures 4.6 and 4.7) at these stages. At planula and primary polyp stage, the expression was observed in the pharynx region, the mesenteries, and (in primary polyps) the mesendodermal tissue of the tentacles. This indicates that the enzymes participate in specific functions within the mesendodermal layer, and that α-DG could be a substrate for their activity. The mesenteries contain a mesendodermal part that includes the retractor muscles, tissue for nutrient storage and (at later stages) the gonads (Steinmetz et al., 2017). The retractor muscle allows the polyps to retract the pharynx and the tentacles into the body cavity for protection. Studies on muscle cells revealed the *Myosin Heavy Chain* (*MyHC1*) gene to be expressed in the retractor and tentacle muscles of *Nematostella* polyps. By comparing *MyHC1* expression pattern in primary polyp stage, there is a striking similarity to the expression of *dystroglycan* with the prominent expression in the mesenteries and tentacle buds (Renfer et al., 2010). The function of *O*-mannosylated α-DG in muscle tissue is quite well studied in other organisms, giving rise to the hypothesis that the DGC may participate in the anchoring of muscle cells to the basement membrane-like extracellular matrix of the mesoglea in the mesenteries. Analysis of the subcellular distribution of Dystroglycan protein could be a next step in addressing a potential role in the musculature. The mesenteries also contain an ectodermal part, the septal filament. This part of the mesenteries contains the gland cells that secrete digestive enzymes (Steinmetz et al., 2017). Epithelium glycosylation and presence of Dystroglycan has been found to participate in gut homeostasis in the intestinal epithelia of humans (Goto et al., 2016) (Driss et al., 2006). Whether glycosylated α-DG has a role in the septal filaments related to their digestive function remains to be analyzed.

5.3 Expression patterns at early developmental stages are compatible with a Dystroglycan-independent function of *O*-mannosylation.

Neither *dystroglycan* nor *dystrobrevin* show expression in scattered ectodermal cells at late gastrula and early planula stages (Figures 4.6 and 4.7). This could mean that POMT1, POMT2

and POMGNT1 have other substrates than Dystroglycan at these stages. Hardly anything is known about other substrates of these glycosyltransferases in animals. The observation that the conserved enzymes are present in the single-celled choanoflagellates, without the presence of *dystroglycan*, suggests that the enzymes can participate in reactions with other substrates besides Dystroglycan and that these substrates are evolutionarily older than Dystroglycan (Bigotti and Brancaccio, 2021). It is tempting to speculate that in the scattered ectodermal cells, POMT1, POMT2 and POMGNT1 modify such ancient substrates. A caveat for this interpretation is that the *in-situ* hybridizations do not exclude the presence of low levels of Dystroglycan in all cells at gastrula and planula stages. It remains therefore uncertain whether Dystroglycan is the only substrate of these enzymes in *Nematostella*.

Hints about the identity of the scattered *POMT1*, *POMT2* and *POMGNT1*-expressing cells come from the observation that *POMGNT1* transcripts are enriched in *FoxQ2d::*mOrange-expressing cells (Rentzsch lab, unpublished data). Using dFISH, we found that at gastrula stage, *POMGNT1* was co-expressed with *FoxQ2d* in at least one typical elongated cell. *FoxQ2d* was also co-expressed with *POMGNT1* in a few roundish cells within the ectoderm, which is typical for cells undergoing mitosis and has been observed previously for *FoxQ2d* (Figure 4.10) (Busengdal and Rentzsch, 2017). Since dFISH showed co-expression of *POMGNT1* with *POMT1* and *POMT2*, there is a high probability that both *POMT1* and *POMT2* would also be expressed in *FoxQ2d*-expressing cells. *FoxQ2d* is expressed in a small population of cells that give rise to putative sensory cells with an elongated cell body and several short basal processes (Busengdal and Rentzsch, 2017). This suggests these enzymes play a role in sensory cells and their progenitors, either with or without their known substrate α-DG. Assuming that Dystroglycan is present in *FoxQ2d*-expressing sensory cells, one could argue that this is related to the importance of Dystroglycan glycosylation in synapses in both the CNS and PNS. Glycosylation of α-DG has been shown to play an important role in synapses, for example in the stability of GABAergic synapses in the cerebral cortex, the formation of ribbon synapses in the retina and clustering of the acetylcholine receptors at the NMJ (Haenggi and Fritschy, 2006; Levi et al., 2002; McMahan et al., 1978; Nickolls and Bonnemann, 2018; Sato et al., 2008). Alternatively, *O*-mannosylation of Dystroglycan or other substrates might affect interactions of the *FoxQ2d*-expressing cells with the extracellular matrix required for their stable integration in the ectodermal epithelium.

5.4 A specific function for *POMGNT1* in cells of the apical organ?

Another interesting observation is the difference in expression pattern between *POMGNT1* and *POMT1/POMT2* in the planula stage. At this stage the presence of *POMGNT1*-expressing cells at the apical organ was observed, corresponding to the identification of *POMGNT1* in the apical organ of *Nematostella* in an earlier study (Sinigaglia et al., 2015). Elevated expression levels of *POMT1* and *POMT2* are not visible in the apical organ, which is surprising given the overall similarity to *POMGNT1*-expression. POMGNT1 modifies substrates after they have been modified by POMT1 and POMT2 and we therefore assume that POMT1 and POMT2 are present in the apical organ, though not at elevated levels. Apical organs are sensory structures found in the larval stage, with a tuft of long cilia, considered to be involved in settlement, locomotion, and metamorphosis (Sinigaglia et al., 2015). At planula stage, the *Nematostella* apical organ is the target of many neurites, which suggests that it has a role in attracting these neurites (Nakanishi et al., 2012). Dystroglycan has been found to have multiple roles in axon guidance where it can function as growth substrate, guidance cues and a stability anchor as neurites cross the basement membrane (Lindenmaier et al., 2019). Whether the Dystroglycan-dependent axon guidance in humans has a connection to neurite attraction of the apical organ in *Nematostella*, is yet unknown, since the function of the apical organ is still not fully deciphered. Whether *POMGNT1* expression in the apical organ proposes a function in the neurite guidance remains unclear, but it is certainly an interesting observation that invites for further studies on the role of *POMGNT1* in the apical organ of *Nematostella.*

5.5 Mutant *POMGNT1*-animals were successfully created by CRISPR/Cas9

To get a closer insight to the function of *POMGNT1* in *Nematostella*, mutants were generated by CRISPR/Cas9. By performing melt curve analysis on gDNA extracted from primary polyp stage, a confirmation of generated mutants was obtained. 4 out of 8 tested animals showed a shift in the derivate slope, thereby confirming changes in the DNA sequence. To further characterize the function of *POMGNT1*, the remaining F0 animals are now raised to sexual maturity before they can be crossed with WT F0 animals. Sequencing of tissue pieces of the new F1 generation would identify the possible heterozygous animals, and in-crosses of these F1 animals would be used to obtain homozygous mutants. As knockout of *POMGNT1* in mice has exhibited extensive abnormalities in the brain such as overmigrating neurons, eye-

defects, reduced muscle mass and stabilization and reduced fertility, similarly severe consequences could be expected in the homozygous mutants (Liu et al., 2010). Due to the generation time of *Nematostella*, the timeline of this master thesis did not allow for this experiment to be carried further.

5.6 Conclusion and future perspectives

The results indicate the presence and necessity of *O*-mannosylation in the development of *Nematostella* at early stages, probably in a cell type-specific manner that includes *FoxQ2d*-expressing neurons. Given the difference in expression pattern between the enzymes and the substrate *dystroglycan* at these early stages, it is possible that the enzymes are linked to other yet- to-be identified substrates than α-DG, or they perform a glycosylation-independent function. The broad mesendodermal expression of the different glycosyltransferases and *dystroglycan* at later developmental stages is compatible with a bilaterian-like role of *O*-mannosylated Dystroglycan in the musculature and in other tissues.

For further studies it would be interesting to repeat the colorimetric ISH with even earlier stages to identify exactly when the individual gene expressions originate. As there are several additional enzymes important for the glycosylation of α-DG, investigating the presence of these within the *Nematostella* genome could be something to consider for future work. The dFISH experiment was also performed on later stages and with other gene combinations than those included in the results, but the experiment did not generate data of good quality. Double FISH experiments certainly must be repeated and expanded to include probes for additional genes, for example genes expressed in additional populations of neurons or in the musculature. Potential co-expression of *dystroglycan* and *fukutin* with the enzymes studied here would also be informative.

To investigate the molecular composition of the Dystroglycan complex in *Nematostella*, studying the protein-protein interactions would be an interesting place to start. By using co-immunoprecipitation, Dystroglycan protein could be isolated together with its interaction partners, and these can be identified. This would require antibodies against *Nematostella*

Dystroglycan or the transgenic expression of a tagged version. Both are currently not available but could be generated.

For the function of *POMGNT1*, homozygous mutants could be used for crossing with transgenic reporter lines, like *FoxQ2d::mOrange* as a marker for sensory neurons or *NvElav1::mOrange*, as a marker for sensory and ganglion neurons. Crossing with the muscle-specific transgenic reporter line *MyHC1::mCherry*, could allow for interesting findings regarding the function of the enzyme and *O*-mannosylation in muscle cells (Renfer et al., 2010). This would allow for better understanding of the relationship between *POMGNT1* and neuronal and other cell types in *Nematostella*. In a broader context, studying the dystrophin-glycoprotein complex in *Nematostella* could provide new insights into the role of cell-ECM interactions for the evolution of neuronal and muscular systems.

6 References

Adams, J.C., Brancaccio, A., 2015. The evolution of the dystroglycan complex, a major mediator of muscle integrity. Biol Open 4, 1163-1179.

Alberts B, J.A., Lewis J, et al, 2002. Molecular Biology of the Cell. 4th edition. Garland Science, New York.

Altschul, S.F., Gish, W., Miller, W., Myers, E.W., Lipman, D.J., 1990. Basic local alignment search tool. J Mol Biol 215, 403-410.

Barros, C.S., Franco, S.J., Müller, U., 2011. Extracellular matrix: functions in the nervous system. Cold Spring Harbor perspectives in biology 3, a005108-a005108.

Bigotti, M.G., Brancaccio, A., 2021. High degree of conservation of the enzymes synthesizing the laminin-binding glycoepitope of alpha-dystroglycan. Open Biol 11, 210104.

Bossert, P.E., Dunn, M.P., Thomsen, G.H., 2013. A staging system for the regeneration of a polyp from the aboral physa of the anthozoan Cnidarian Nematostella vectensis. Dev Dyn 242, 1320-1331.

Burton, P.M., Finnerty, J.R., 2009. Conserved and novel gene expression between regeneration and asexual fission in Nematostella vectensis. Dev Genes Evol 219, 79-87.

Busengdal, H., Rentzsch, F., 2017. Unipotent progenitors contribute to the generation of sensory cell types in the nervous system of the cnidarian Nematostella vectensis. Dev Biol 431, 59-68.

Darling, J.A., Reitzel, A.M., Finnerty, J.R., 2004. Regional population structure of a widely introduced estuarine invertebrate: Nematostella vectensis Stephenson in New England. Mol Ecol 13, 2969-2981.

Diesen, C., Saarinen, A., Pihko, H., Rosenlew, C., Cormand, B., Dobyns, W.B., Dieguez, J., Valanne, L., Joensuu, T., Lehesjoki, A.E., 2004. POMGnT1 mutation and phenotypic spectrum in muscle-eye-brain disease. J Med Genet 41, e115.

Driehuis, E., Clevers, H., 2017. CRISPR/Cas 9 genome editing and its applications in organoids. Am J Physiol Gastrointest Liver Physiol 312, G257-G265.

Driss, A., Charrier, L., Yan, Y., Nduati, V., Sitaraman, S., Merlin, D., 2006. Dystroglycan receptor is involved in integrin activation in intestinal epithelia. American Journal of Physiology-Gastrointestinal and Liver Physiology 290, G1228-G1242.

Endo, T., 2007. Dystroglycan glycosylation and its role in alpha-dystroglycanopathies. Acta Myol 26, 165-170.

Endo, T., 2014. Glycobiology of α-dystroglycan and muscular dystrophy. The Journal of Biochemistry 157, 1-12.

Endo, T., 2015. Glycobiology of alpha-dystroglycan and muscular dystrophy. J Biochem 157, 1-12.

Fritzenwanker, J.H., Genikhovich, G., Kraus, Y., Technau, U., 2007. Early development and axis specification in the sea anemone Nematostella vectensis. Dev Biol 310, 264-279.

Fritzenwanker, J.H., Technau, U., 2002. Induction of gametogenesis in the basal cnidarian Nematostella vectensis (Anthozoa). Dev Genes Evol 212, 99-103.

Galliot, B., Schmid, V., 2002. Cnidarians as a model system for understanding evolution and regeneration. Int J Dev Biol 46, 39-48.

Gomez Toledo, A., Raducu, M., Cruces, J., Nilsson, J., Halim, A., Larson, G., Rüetschi, U., Grahn, A., 2012. O-Mannose and O–N-acetyl galactosamine glycosylation of mammalian α-dystroglycan is conserved in a region-specific manner. Glycobiology 22, 1413-1423.

Goto, Y., Uematsu, S., Kiyono, H., 2016. Epithelial glycosylation in gut homeostasis and inflammation. Nature Immunology 17, 1244-1251.

Grewal, P.K., Holzfeind, P.J., Bittner, R.E., Hewitt, J.E., 2001. Mutant glycosyltransferase and altered glycosylation of alpha-dystroglycan in the myodystrophy mouse. Nat Genet 28, 151-154.

Haenggi, T., Fritschy, J.M., 2006. Role of dystrophin and utrophin for assembly and function of the dystrophin glycoprotein complex in non-muscle tissue. Cell Mol Life Sci 63, 1614-1631.

Hand, C., Uhlinger, K.R., 1992. The Culture, Sexual and Asexual Reproduction, and Growth of the Sea-Anemone Nematostella-Vectensis. Biol Bull 182, 169-176.

Hartenstein, V., Stollewerk, A., 2015. The evolution of early neurogenesis. Dev Cell 32, 390-407.

Hayashi, Y.K., Ogawa, M., Tagawa, K., Noguchi, S., Ishihara, T., Nonaka, I., Arahata, K., 2001. Selective deficiency of alpha-dystroglycan in Fukuyama-type congenital muscular dystrophy. Neurology 57, 115-121.

Henry, M.D., Campbell, K.P., 1998. A role for dystroglycan in basement membrane assembly. Cell 95, 859-870.

Hobert, O., Kratsios, P., 2019. Neuronal identity control by terminal selectors in worms, flies, and chordates. Current Opinion in Neurobiology 56, 97-105.

Hobro, A.J., Smith, N.I., 2017. An evaluation of fixation methods: Spatial and compositional cellular changes observed by Raman imaging. Vib Spectrosc 91, 31-45.

Holstein, T.W., Hobmayer, E., Technau, U., 2003. Cnidarians: an evolutionarily conserved model system for regeneration? Dev Dyn 226, 257-267.

Hrdina, P.D., 1996. Basic neurochemistry: Molecular, cellular and medical aspects - Siegel,GJ. J Psychiatr Neurosci 21, 352-353.

Hua, R.F., Yu, S.S., Liu, M.G., Li, H.H., 2018. A PCR-Based Method for RNA Probes and Applications in Neuroscience. Front Neurosci-Switz 12.

Ichimiya, T., Manya, H., Ohmae, Y., Yoshida, H., Takahashi, K., Ueda, R., Endo, T., Nishihara, S., 2004. The twisted abdomen phenotype of Drosophila POMT1 and POMT2 mutants coincides with their heterophilic protein O-mannosyltransferase activity. Journal of Biological Chemistry 279, 42638-42647.

Imae, R., Manya, H., Tsumoto, H., Osumi, K., Tanaka, T., Mizuno, M., Kanagawa, M., Kobayashi, K., Toda, T., Endo, T., 2018. CDP-glycerol inhibits the synthesis of the functional O-mannosyl glycan of alpha-dystroglycan. J Biol Chem 293, 12186-12198.

Kelava, I., Rentzsch, F., Technau, U., 2015. Evolution of eumetazoan nervous systems: insights from cnidarians. Philos T R Soc B 370.

Kessler, C., 1994. Nonradioactive Analysis of Biomolecules. J Biotechnol 35, 165-189.

Layden, M.J., Boekhout, M., Martindale, M.Q., 2012. Nematostella vectensis achaete-scute homolog NvashA regulates embryonic ectodermal neurogenesis and represents an ancient component of the metazoan neural specification pathway. Development 139, 1013-1022.

Layden, M.J., Martindale, M.Q., 2014. Non-canonical Notch signaling represents an ancestral mechanism to regulate neural differentiation. Evodevo 5, 30.

Layden, M.J., Rentzsch, F., Rottinger, E., 2016. The rise of the starlet sea anemone Nematostella vectensis as a model system to investigate development and regeneration. Wires Dev Biol 5, 408-428.

Lee, K.J., Jessell, T.M., 1999. The specification of dorsal cell fates in the vertebrate central nervous system. Annu Rev Neurosci 22, 261-294.

Lee, P.N., Kumburegama, S., Marlow, H.Q., Martindale, M.Q., Wikramanayake, A.H., 2007. Asymmetric developmental potential along the animal-vegetal axis in the anthozoan cnidarian, Nematostella vectensis, is mediated by Dishevelled. Dev Biol 310, 169-186.

Levi, S., Grady, R.M., Henry, M.D., Campbell, K.P., Sanes, J.R., Craig, A.M., 2002. Dystroglycan is selectively associated with inhibitory GABAergic synapses but is dispensable for their differentiation. J Neurosci 22, 4274-4285.

Lindenmaier, L.B., Parmentier, N., Guo, C.Y., Tissir, F., Wright, K.M., 2019. Dystroglycan is a scaffold for extracellular axon guidance decisions. Elife 8.

Liu, J., Yang, Y., Li, X., Zhang, P., Qi, Y., Hu, H., 2010. Chapter Twenty - Cellular and Molecular Characterization of Abnormal Brain Development in Protein O-Mannose N-Acetylglucosaminyltransferase 1 Knockout Mice, in: Fukuda, M. (Ed.), Methods in Enzymology. Academic Press, pp. 353-366.

Lodish H, B.A., Zipursky SL, et al., 2016. Molecular Cell Biology. W. H. Freeman and Company, New York.

Lommel, M., Strahl, S., 2009. Protein O-mannosylation: Conserved from bacteria to humans*. Glycobiology 19, 816-828.

Long, K.R., Huttner, W.B., 2019. How the extracellular matrix shapes neural development. Open Biol 9, 180216.

Lovinger, D.M., 2008. Communication networks in the brain: neurons, receptors, neurotransmitters, and alcohol. Alcohol Res Health 31, 196-214.

Manya, H., Chiba, A., Yoshida, A., Wang, X., Chiba, Y., Jigami, Y., Margolis, R.U., Endo, T., 2004. Demonstration of mammalian protein O-mannosyltransferase activity: Coexpression of POMT1 and POMT2 required for enzymatic activity. P Natl Acad Sci USA 101, 500-505.

Manya, H., Sakai, K., Kobayashi, K., Taniguchi, K., Kawakita, M., Toda, T., Endo, T., 2003. Loss-of-function of an N-acetylglucosaminyltransferase, POMGnT1, in muscle-eye-brain disease. Biochem Bioph Res Co 306, 93-97.

McMahan, U.J., Sanes, J.R., Marshall, L.M., 1978. Cholinesterase is associated with the basal lamina at the neuromuscular junction. Nature 271, 172-174.

Moiseeva, E., Rabinowitz, C., Paz, G., Rinkevich, B., 2017. Histological study on maturation, fertilization and the state of gonadal region following spawning in the model sea anemone, Nematostella vectensis. PLoS One 12, e0182677.

Montanaro, F., Carbonetto, S., 2003. Targeting dystroglycan in the brain. Neuron 37, 193-196.

Monzo, P., Crestani, M., Chong, Y.K., Ghisleni, A., Hennig, K., Li, Q., Kakogiannos, N., Giannotta, M., Richichi, C., Dini, T., Dejana, E., Maiuri, P., Balland, M., Sheetz, M.P., Pelicci, G., Ang, B.T., Tang, C., Gauthier, N.C., 2021. Adaptive mechanoproperties mediated by the formin FMN1 characterize glioblastoma fitness for invasion. Dev Cell 56, 2841-2855 e2848.

Nakanishi, N., Renfer, E., Technau, U., Rentzsch, F., 2012. Nervous systems of the sea anemone Nematostella vectensis are generated by ectoderm and endoderm and shaped by distinct mechanisms. Development 139, 347-357.

Nickolls, A.R., Bonnemann, C.G., 2018. The roles of dystroglycan in the nervous system: insights from animal models of muscular dystrophy. Dis Model Mech 11.

Nordberg, H., Cantor, M., Dusheyko, S., Hua, S., Poliakov, A., Shabalov, I., Smirnova, T., Grigoriev, I.V., Dubchak, I., 2014. The genome portal of the Department of Energy Joint Genome Institute: 2014 updates. Nucleic Acids Res 42, D26-31.

Panin, V.M., Wells, L., 2014. Protein O-mannosylation in metazoan organisms. Curr Protoc Protein Sci 75, 12 12 11-12 12 29.

Paridaen, J.T.M.L., Huttner, W.B., 2014. Neurogenesis during development of the vertebrate central nervous system. EMBO Rep 15, 351-364.

Prada, J., Castellanos, J., 2013. Real time PCR. Application in dengue studies. Colombia Medica 42, 243-258.

Putnam, N.H., Srivastava, M., Hellsten, U., Dirks, B., Chapman, J., Salamov, A., Terry, A., Shapiro, H., Lindquist, E., Kapitonov, V.V., Jurka, J., Genikhovich, G., Grigoriev, I.V., Lucas, S.M., Steele, R.E., Finnerty, J.R., Technau, U., Martindale, M.Q., Rokhsar, D.S., 2007. Sea anemone genome reveals ancestral eumetazoan gene repertoire and genomic organization. Science 317, 86-94.

Quan, X.J., Hassan, B.A., 2005. From skin to nerve: flies, vertebrates and the first helix. Cell Mol Life Sci 62, 2036-2049.

Reitzel, A.M., Burton, P.M., Krone, C., Finnerty, J.R., 2007. Comparison of developmental trajectories in the starlet sea anemone Nematostella vectensis: embryogenesis, regeneration, and two forms of asexual fission. Invertebr Biol 126, 99-112.

Renfer, E., Amon-Hassenzahl, A., Steinmetz, P.R.H., Technau, U., 2010. A muscle-specific transgenic reporter line of the sea anemone, Nematostella vectensis. P Natl Acad Sci USA 107, 104-108.

Rentzsch, F., Layden, M., Manuel, M., 2017. The cellular and molecular basis of cnidarian neurogenesis. Wires Dev Biol 6.

Rentzsch, F., Renfer, E., Technau, U., 2020. Generating Transgenic Reporter Lines for Studying Nervous System Development in the Cnidarian Nematostella vectensis. Methods Mol Biol 2047, 45-57.

Richards, G., Rentzsch, F., 2015. Regulation of Nematostella neural progenitors by SoxB, Notch and bHLH genes. Development 142, 3332-3342.

Richards, G.S., Rentzsch, F., 2014. Transgenic analysis of a SoxB gene reveals neural progenitor cells in the cnidarian Nematostella vectensis. Development 141, 4681-4689.

Röttinger, E., 2021. Nematostella vectensis, an Emerging Model for Deciphering the Molecular and Cellular Mechanisms Underlying Whole-Body Regeneration. Cells 10.

Sato, S., Omori, Y., Katoh, K., Kondo, M., Kanagawa, M., Miyata, K., Funabiki, K., Koyasu, T., Kajimura, N., Miyoshi, T., Sawai, H., Kobayashi, K., Tani, A., Toda, T., Usukura, J., Tano, Y., Fujikado, T., Furukawa, T., 2008. Pikachurin, a dystroglycan ligand, is essential for photoreceptor ribbon synapse formation. Nat Neurosci 11, 923-931.

Schindelin, J., Arganda-Carreras, I., Frise, E., Kaynig, V., Longair, M., Pietzsch, T., Preibisch, S., Rueden, C., Saalfeld, S., Schmid, B., Tinevez, J.-Y., White, D.J., Hartenstein, V., Eliceiri, K., Tomancak, P., Cardona, A., 2012. Fiji: an open-source platform for biological-image analysis. Nature Methods 9, 676-682.

Sinigaglia, C., Busengdal, H., Lerner, A., Oliveri, P., Rentzsch, F., 2015. Molecular characterization of the apical organ of the anthozoan Nematostella vectensis. Dev Biol 398, 120-133.

Sparks, S.E., 2012. Congenital protein hypoglycosylation diseases. Appl Clin Genet 5, 43-54.

Squire, L.R., Berg, D., Bloom, F.E., du Lac, S., Ghosh, A., Spitzer, N.C., 2008. Fundamental Neuroscience, in: Squire, L.R., Berg, D., Bloom, F.E., du Lac, S., Ghosh, A., Spitzer, N.C. (Eds.), Fundamental Neuroscience (Third Edition). Academic Press, San Diego.

Steinmetz, P., Aman, A., Kraus, J., Technau, U., 2017. Gut-like ectodermal tissue in a sea anemone challenges germ layer homology. Mech Develop 145, S111-S111.

Technau, U., 2020. Gastrulation and germ layer formation in the sea anemone Nematostella vectensis and other cnidarians. Mech Develop 163.

Technau, U., Steele, R.E., 2011. Evolutionary crossroads in developmental biology: Cnidaria. Development 138, 1447-1458.

Telford, Maximilian J., Budd, Graham E., Philippe, H., 2015. Phylogenomic Insights into Animal Evolution. Current Biology 25, R876-R887.

Tournière, O., 2020. Specification and differentiation of neural cells in *Nematostella vectensis.*, Department of Biological Sciences. The University of Bergen, p. 96.

Tournière, O., Dolan, D., Richards, G.S., Sunagar, K., Columbus-Shenkar, Y.Y., Moran, Y., Rentzsch, F., 2020. NvPOU4/Brain3 Functions as a Terminal Selector Gene in the Nervous System of the Cnidarian Nematostella vectensis. Cell Reports 30, 4473-4489.e4475.

Uribe, M.L., Haro, C., Ventero, M.P., Campello, L., Cruces, J., Martin-Nieto, J., 2016. Expression pattern in retinal photoreceptors of POMGnT1, a protein involved in muscle-eye-brain disease. Mol Vis 22, 658-673.

Waite, A., Brown, S.C., Blake, D.J., 2012. The dystrophin-glycoprotein complex in brain development and disease. Trends Neurosci 35, 487-496.

Watanabe, H., Fujisawa, T., Holstein, T.W., 2009. Cnidarians and the evolutionary origin of the nervous system. Dev Growth Differ 51, 167-183.

Watanabe, H., Kuhn, A., Fushiki, M., Agata, K., Özbek, S., Fujisawa, T., Holstein, T.W., 2014. Sequential actions of β-catenin and Bmp pattern the oral nerve net in Nematostella vectensis. Nature Communications 5, 5536.

Wells, L., 2013. The o-mannosylation pathway: glycosyltransferases and proteins implicated in congenital muscular dystrophy. The Journal of biological chemistry 288, 6930-6935.

Williams, R.B., 1975. A redescription of the brackish-water sea anemone Nematostella vectensis Stephenson, with an appraisal of congeneric species. Journal of Natural History 9, 51-64.

Xin, X., Akasaka-Manya, K., Manya, H., Furukawa, J., Kuwahara, N., Okada, K., Tsumoto, H., Higashi, N., Kato, R., Shinohara, Y., Irimura, T., Endo, T., 2015. POMGNT1 Is Glycosylated by Mucin-Type O-Glycans. Biological & Pharmaceutical Bulletin 38, 1389-1394.

Xiong, H., Kobayashi, K., Tachikawa, M., Manya, H., Takeda, S., Chiyonobu, T., Fujikake, N., Wang, F., Nishimoto, A., Morris, G.E., Nagai, Y., Kanagawa, M., Endo, T., Toda, T., 2006. Molecular interaction between fukutin and POMGnT1 in the glycosylation pathway of α-dystroglycan. Biochem Bioph Res Co 350, 935-941.

Zhao, D., Chen, S.Y., Liu, X., 2019. Lateral neural borders as precursors of peripheral nervous systems: A comparative view across bilaterians. Dev Growth Differ 61, 58-72.